Author Response to Reviews of

Which processes drive observed variations of HCHO columns over India?

Luke Surl, Paul I. Palmer, and Gonzalo González Abad
Atmospheric Chemistry and Physics Discussions, doi:10.5194/acp-2017-1017

RC: ***Reviewer Comment***, AR: *Author Response*, ☐ Manuscript text

We thanks the reviewers for their careful readings of the manuscript and suggestions for improvement. This document details our responses to these and the subsequent changes we have made to the revised manuscript.

1. Reviewer #1

1.1. General comment #1

RC: ***Indicate the locations of geographic features in India on the Figures provided so that it is easy for someone not familiar with the country to follow along. For example, locations of the Thar Desert, the IGP, and the five megacities should be provided in Figure 1 (Lines 50-52), the features referred to in lines 310-315 should be indicated in Figure 5, and the features referred to in lines 292-293 should be located on the plot (in particular Rann of Kutch).***

AR: *We have added labels to these figures to assist the reader in locating these features.*

1.2. General comment #2

RC: ***In the list of methods applied to deriving isoprene emissions (Lines 85-90), the local NOx dependent relationship used in Marais et al. (2012) in missing. The authors point out that the correlations and slopes obtained in each season between HCHO and isoprene emissions in GEOS-Chem are highly variable. What drives this variability? Is it NOx? Would it be more effective then to use a NOx-dependent HCHO yield to derive isoprene emissions from OMI HCHO?***

AR: *Not including Marais et al (2012) here was an egregious oversight. At least some of the uncertainty in our linearized isoprene emissions will have been caused by variations in HCHO yields due to its sensitivity to NOx. Certainly, over India our understanding of NOx emissions is highly uncertain so we felt it was not appropriate to use this method. Nevertheless, we have included text to acknowledge and explain the benefits of the Marais method:*

> *For central Africa, Marais et al (2012) employed an inversion method that accounted for the NOx-dependence of the isoprene-HCHO relationship*

1.3. General comment #3

RC: ***Why when comparing the multiyear average and year-to-year variability of OMI HCHO to the 2014 values is OMI HCHO for 2008-2015 used? Why not use the full OMI HCHO record starting from the first complete year (i.e. 2005-2015)?***

AR: *The purpose of this exercise was not to show the whole time series but rather to show that 2014 is representative of the previous few years. As Mahahjan et al 2015 showed that there was a long-term trend to the HCHO columns over India, we determined extending this comparison further back had the potential for causing confusion.*

1.4. General comment #4

RC: ***What drives the year-to-year variability in HCHO (Figure 7, Line 22)?***

AR: *This is a good question but not the main focus of this current analysis. We wanted to understand whether our study year (2014) was representation of a longer time period. It seems from our analysis that 2014 was not anomalous. However, based on our analysis it seems that surface temperature is a good predictor for continental-scale variations of OMI slant columns of HCHO. For a more detailed analysis of the drivers we refer the reader to Mahahjan et al 2015.*

> *Mahajan et al. (2015) reports an analysis of the drivers of year-to-year variations in HCHO columns over India.*

1.5. General comment #5

RC: ***Some information regarding the isoprene oxidation chemistry in each model is needed so that the reader can assess whether the 2 models (CAABA and GEOS-Chem) have the same isoprene oxidation chemistry, or whether CAABA, due to lower computational needs than a 3D model, has a more detailed representation of isoprene oxidation than GEOS-Chem. Have both models kept pace with new findings of isoprene oxidation mechanisms reported in the literature? Are NOx-dependent HCHO yields from isoprene oxidation similar for the 2 models?***

AR: *The mechanisms are not the same. We have added text referring the reader to studies where both GEOS-Chem and MIM2 (the mechanism used in the box model) are compared to the Master Chemical Mecahnism and their HCHO-related chemistry results are assessed.*

> The chemical mechanisms from the CAABA box model and the GEOS-Chem model are not identical. CAABA includes a more explicit chemical mechanism and a reduced version of the Mainz Isoprene Mechanism 2 (MIM2, Taraborelli et al, 2009). The version of GEOS-Chem we use here is described by Eastham et al, 2014. The latest version of the GEOS-Chem chemical mechanism, released after the majority of our calculations had been completed, results in an increase of the HCHO yield from the oxidation of isoprene. We find using preliminary calculations with v11.01 that the revised mechanism does not systematically change the results shown here. Previous studies have evaluated the performance of GEOS-Chem (Marvin et al, 2017) and MIM2 (Taraborelli et al, 2009) against the Master Chemical Mechanism. The GEOS-Chem v10.01 mechanism slightly underestimates HCHO production in high-NOx conditions and the MIM2 mechanism shows similar HCHO production across a wide range of NOx values.

1.6. General comment #6

RC: ***The manuscript is missing a Data Availability section (`https://www.atmospheric-chemistry-and-physics.net/about/data_policy.html`).***

AR: *We have added a data availability section to the revised manuscript*

1.7. Specific comments and typographical errors

All of the comments which relate to simple typographical errors have been fixed as per the reviewer's recommendation.

RC: ***Line 11: "comparable (slower)" is contradictory. Which is it? -***

AR: *We mean with this line to indicate that the values are comparable but slightly slower. We have changed this to "but slower" to improve clarity here.*

RC: ***Lines 69-71: Please specify whether these trends in HCHO are for large urban areas, rural regions or across the country.***

AR: *These values are for the whole country. This has been clarified in the text*

RC: ***Line 186-187: "30 in the troposphere" is appropriate for a fixed tropopause, but doesn't the model have a dynamic tropopause that leads to variability in the number of levels in the troposphere?***

AR: *The reviewer is right that GEOS-Chem has a dynamic tropopause. We have changed the text to:*

> *of which about 30 are normally below the dynamic tropopause*

RC: ***Line 195: Is MIX a mosaic of regional inventories? As written this isn't clear.***

AR: *The reviewer is correct that MIX is a mosaic of regional inventories. We have clarified that we are talking about the output from this mosaic in this sentence.*

RC: ***Line 201: Provide the version of MEGAN that is used***

AR: *We have added the version number (v2.1)*

RC: ***Lines 206-207: Say where the drivers of MEGAN are from. Is LAI from the model fields or from MODIS?***

AR: *We have added text to state that MEGANv2.1 uses MODIS LAI.*

RC: ***Line 297: The meaning of the 11% is not clear. Is 11% the percent increase in vertical columns relative to slant columns after applying the AMF? Or is this an increase in the spatial correlation after applying the AMF?***

AR: *This 11% value is derived from a comparison of the correlation coefficients. This is made clear in the revised text.*

RC: ***Lines 347-348: Reiterate that the slant columns are used for 2008-2015.***

AR: *This reiteration has been added as suggested.*

RC: ***Line 352: Should "Median" be mean? That's what's shown in Figure 8.***

AR: *The term "median" is used correctly here. While mean values are better for the graphics, for this particular statistic the median value is more useful as it is not perturbed by a handful of likely erroneous extremes.*

RC: ***Line 384: Don't mature leaves emit more isoprene than young and senescing leaves (Guenther et al.,***

2006)? This sentence needs to be revised to reflect that.

AR: *This sentence was unclear in the original manuscript. We have replaced it with this sentence:*

> *Thermotolerance is one hypothesis that describes why leaves emit isoprene (Singaas et al., 1997). After a few weeks of emerging, the emission capacity of leaves peaks and subsequently declines with age.*

RC: ***Lines 424-425: Why does the bottom-up emission inventory overestimate emissions from the transport sector when the inventory is for 2010 and the simulation year is 2014? Wouldn't this misrepresent the growth in this sector and so underestimate emissions from the transport sector? The reasoning for an overestimate is not immediately clear***

AR: *The expectation of a decrease in transport emissions 2010-2014 assumes transportation is emitting less VOC per unit as engines are modernized and regulations come into force.*

RC: ***Line 456: Are the "sample mean" and "sample standard deviation" the regional mean and standard deviation of column HCHO for the whole country? If so, please clarify this in the text.***

AR: *We have clarified that the datasets here are for the whole country.*

RC: ***Line 461: Rather than stating that further work is "outside the scope of this current study", more impactful to point out that this is an early demonstration of the efficacy of future geostationary satellites that will provide constraints on the temporal variability of HCHO.***

AR: *We have changed this to*

> *and is an early demonstration of how datasets with continuous measurements for a region (such as those from a geostationary satellite) could help constrain the temporal variability of HCHO*

1.8. Comments on Figures and Tables

RC: ***Figure 1: • City names (perhaps capital cities?) and the legend in the population map are not legible. • The population map has a panel header ("India Population Map"). The other panels would benefit from headers too. • The red outline could be made clearer in the top right map***

AR: *Figure 1A (the population map) has been replaced.*

Headers have been added to these figures.

RC: ***Figure 2: • Label "C" is missing. • Consider choosing a colour bar with a more dynamic colour range. As is, JJAS emissions seem only marginally higher than emissions in other months. • What are the isoprene emission units? "g C", "molecules C", or "mg C"?***

AR: *The missing label has been added. The color bar as been clarified as atoms C/cm2/s. As listed in Table 3, it is the MAM isoprene emissions which are generally higher rather than JJAS, and we feel the color scale on Figure 2 shows this adequately.*

RC: ***Figure 3: Consider including initial NOx (or NO) concentrations for each isoprene HCHO yield line shown in the plot.***

AR: *We feel this information is better presented in a tabular format, the NO_2 ratios are present in Table 1. We have revised text in the manuscript to better highlight these values.*

RC: ***Figure 7: • "Left" should be "top" and "right" should be "bottom" in the figure caption.***

AR: *The caption has been corrected.*

RC: ***Figure 9: • Consider choosing a colour bar with a more dynamic colour range***

AR: *The choice of a color bar with maximum at 1ppb is deliberate, as this shows that for almost all of India the "High NOx" conditions are likely. Variations above 1ppb are less important than those around the 0.1ppb range.*

RC: ***Figure 12: • Labels on the map are not legible. • Consider replacing "map imagery" with "road network".***

AR: *The caption has been changed as suggested. The underlying road network image has been changed to one that is clearer.*

RC: ***Table 1: • Include a footnote in the table to indicate the source of variables (T, RH, BLH, O3, CO, NO2) provided.***

AR: *The footnote has been added as suggested*

2. Reviewer #2

2.1. Major comment 1

RC: ***Version 10-01 of the GEOS-Chem model is used in this analysis. The mechanism in v11-01 (released Feb 2017) includes large revisions on the isoprene oxidation mechanism effecting the HCHO yield. Specifically, the prompt yield of HCHO from the reaction of the isoprene peroxy radical with NO (RIO2 + NO) is increased by 24% (from 0.66 to 0.82). The revised mechanism is in good agreement with fully explicit mechanisms and generally reproduces observations (Marvin et al., 2017). Because we have more confidence in the updated mechanism, and because the mechanism is likely to affect the modeled HCHO columns shown here, the updated isoprene oxidation mechanism should be used in this analysis.***

AR: *The reviewer correctly notes that the isoprene oxidation mechanism has revised in the transition from GEOS-Chem v10-01 (used in this study) and v11-01 which was released in early 2017. The model calculations used in this project were initiated prior to the release of v11-01.*

We have recently installed GEOS-Chem v11-01. Re-doing the all calculations of this manuscript with a new model would not be viable in the normal turnaround time for a revised paper in ACP. Instead, to assess the likely impact of the difference in mechanism, we have compared model results for a test case month (April 2014).

For this test case, the model output was, in terms of HCHO columns, both qualitatively and quantitatively, similar for both versions of the model. There are no features in the model output for v11 that are not present in v10 (and vice versa). The model output vertical HCHO columns were strongly correlated without significant bias between them ([v11] = 0.96[v10] + 0.6×10^{15}, r^2 = 0.89). We decided not to include this in that manuscript.

2.2. Major comment 2

RC: ***It is unclear here if the chemical mechanism used in the CABBA/MECA box model is the same as used in the GEOS-Chem simulation. Ideally, the same mechanisms would be used.***

AR: *The mechanisms are not the same. The mechanism used in GEOS-Chem is the NOx-Ox-HC-Aer-Br (a.k.a. "tropchem") mechanism which was in the standard release of GEOS-Chem v10-01. Text has been added directing the reader to Eastham et al (2014) (`http://doi.org/10.1016/j.atmosenv.2014.02.001`) which details the mechanism.*

We have clarified the box model mechanism is the full chemistry as described in Sander et al 2011 and the model's documentation, but without halogen, sulphur and mercury reactions. Additionally, the reader is directed to Taraborelli et al (2009) (`https://doi.org/10.5194/acp-9-2751-2009`) which discusses the "MIM2" isoprene mechanism used in the box model.

We note that, with respect to isoprene chemistry, both GEOS-Chem's chemical mechanism and MIM2 (used in the box model) are evaluated against the Master Chemical Mechamism (MCM) v2.1 in, Marvin et al 2017 and Tamborelli et al 2009 respectively and both generally performed well in reproducing the MCM results. We direct readers interested in this chemistry to these papers, and summarise that, while both comparisons are generally favourable when assessed against MCM, Marvin et al. (2017) finds that GEOS-Chem's mechanism slightly underestimates HCHO production in high-NOx conditions, whereas Tamborelli et al (2009) showed generally similar HCHO-results across the whole NOx range.

Please also note our response to Reviewer 1 above (1.5) that describes the text we have included.

2.3. Major comment 3

RC: ***Recently, Zhu et. al (2016) found that the OMI SAO HCHO product used here was biased low by 37% compared to observations over the Southeastern United States. Do we have any reason to suspect that this bias may persist in other regions of the globe? I understand that in-situ HCHO observations are likely limited for this region; however, acknowledgement of the potential for bias and the need for validation is warranted.***

AR: *Unfortunately, it is not possible for us to evaluate whether a similar bias exists over India due to a lack of in situ data. To inform the reader about this potential bias in OMI we have added a reference to Zhu et al 2016 and a brief summary of their result. Specifically, we have included the following sentences:*

> *"Previous work using aircraft observations over Southeastern United States has shown that the OMHCHOv0003 OMI HCHO column data product has a low bias (37%), and that the GEOS-Chem model v9.02 had a 10% low bias (Zhu et al, 2016). In the absence of similar data over India, we cannot determine with certainty the generality of these biases, and have chosen to implicitly assume that the OMI data are not significantly impacted by systematic error.*

2.4. Minor comments and typographical errors

All of the comments which relate to simple typographical errors have been fixed as per the reviewer's recommendation.

RC: ***Page 3, line 79: It is unclear what is meant by "this approach".***

AR: *This point has now been clarified. "Approach" has been changed to "relationship"*

RC: ***Page 3, sentence starting at line 88: Wolfe et al. (2016) is cited as a reference for the uncertainty in HCHO production in the low NOx regime. In contrast, I think this paper suggests that the NOx dependency of HCHO production is well captured by updated chemical mechanisms. In any case, it is not clear to me why uncertainty in VOC emissions and in the low NOx yield means "both approaches provide useful insights". Perhaps it is more useful to point out that while the inverse model approach gives a more rigorous result, it comes at a higher computational expensive, and the local linear approach provides a useful approximation where there is little smearing.***

AR: *The reviewer is correct that one of the principal advantages of the local linear approach is its lower computational expense. We feel that a comparison of the relative merits of the available approaches would not improve the readability of the manuscript. We already provide a number of references in this paragraph that cover the different methods. This also includes the Marais reference that was missing in the submitted version of the paper.*

RC: ***Page 7, line 201: List which version of MEGAN.***

AR: *We have included the version number (v2.1).*

RC: ***Page 7, line 213: GEOS-Chem HCHO columns are averaged between 1300 and 1500 to provide comparison with OMI observations. Is this a hold-over from GEOS-Chem simulations run at coarse resolution with longer (60 min) timesteps? At the 10 minute chemistry timestep often used for 0.25 x 0.3125 simulations, I would have expected the output to be averaged over a smaller time frame (1300 to 1400). Perhaps the effect is small, but Is there a reason for the 1300 – 1500 averaging window? What are the chemistry and transport time steps used in this simulation?***

AR: *Due to the nature of the satellite orbit the local solar time at overpass can vary by over two hours, which is the reason for this wide averaging window. We found that due to the wide range of longitudes in a single swath, there is a range of approximately 100 minutes in local solar time for the pixels. This provides the motivation for adopting a two-hour window.*

In the high resolution run the transport timestep was 5 minutes and the chemistry timestep was 10 minutes. These values have been added to the text.

RC: ***Page 8, lines 240-226. The box model analysis of isoprene oxidation as a function of NOx seems redundant with other recent publications, which also have the benefit of comparison to in-situ observations (Wolfe et al., 2016; Marvin et al., 2017). For example, figure 3 is reminiscent of Figure S3 in Marvin et al. 2017. At the very least, the box model results here should be compared with those in previous literature.***

AR: *Including the HCHO production from the oxidation of isoprene in Figure 3 was primarily intended to put into context the HCHO production from the oxidation of anthropogenic VOCs. With this figure we were updating a figure published in Palmer 2003 (*`http://doi.org/10.1029/2002JD002153`*) but in this current paper we have linked each calculation with the photochemical environment associated with each Indian forest. We do not wish to directly compare these results to those in dedicated studies of the HCHO yield–NOx relationship as these are qualitatively different exercises (in particular, our study adjusts many variables between model runs, not just NOx). Marvin et al (2017) has been added to the list of previous studies. We have added the following text at the end of the section:*

> The simulations reported in this work are intended to be specific to the Indian scenarios discussed.

RC: ***Page 11, line 370: add a section refence (i.e. "as described in section 2.2")***

AR: *This section reference has been added as per the reviewer's suggestion.*

RC: ***Page 15, lines 491: The procedure of deriving a posteriori emissions using the linear approach should be briefly described for readers unfamiliar with the process.***

AR: *We have added the following text:*

> *We resolve seasonal a priori emissions of isoprene from observed HCHO columns by transposing the model linear relationship between isoprene emissions and HCHO columns.*

AR: *Page 38, Table 3: Consider adding a "% change" column*

RC: ***This has been added as per the reviewer's suggestion.***

3. List of changes

The following is a list of all the changes made in the document. Line numbers refer to the positions in the manuscript appended to this document with highlighted changes

- ***Line 3: "spatial" changed to "horizontal"***
- ***Line 8: "neighbors" changed to "neighbour"***
- ***Line 11: Added "but" before "slower"***
- ***Line 12 and 22: Minor changes regarding hyphens***
- ***Line 22: removed "but there are large year to year variations"***
- ***Line 24: removed "only"***
- ***Line 25: changed "during March to April" to "only during March and April"***
- ***Line 66 and 108: contracted "Ozone Monitoring Instrument" to "OMI"***
- ***Line 71: added "nationwide"***
- ***Line 75: added "by"***
- ***Line 77: added "these" before "data"***
- ***Line 80: changed "approach" to "relationship". Please noted that the highlighting that suggests references have been removed from this line is due to a minor bug and is incorrect.***
- ***Line 86: Added text referring to Marais et al (2012).***
- ***Line 90: changed "NO" to "NO_x"***
- ***Line 140: changed "detailed" to "detail"***
- ***Line 151: added paragraph referring to work of Zhu et al (2016).***
- ***Line 164: added paragraph regarding model mechanisms.***
- ***Line 176: added "but without halogen, sulphur, and mercury chemistry"***
- ***Line 180: corrected citation format.***
- ***Line 203: changed "signal-levels" to "sigma-levels"***
- ***Line 204: changed to "of which about 30 are typically below the dynamic tropopause"***
- ***Line 205: added sentence regarding mechanism***
- ***Line 211: added sentence discussing to inventories. This replaces text from Line 230 which has been removed.***
- ***Line 214: added "mosaic"***

- ***Line 215: removed repeated word***
- ***Line 222: added version number***
- ***Line 236: removed "Due to computational limitations..." sentence.***
- ***Line 272: changed "(>1 ppbv)" to "(averages generally around or above 1 ppbv)"***
- ***Line 275: changed "getting oxidised" to "oxidation"***
- ***Line 282: added "(c.f. NO_2 mixing ratios in Table 1 and yields reported in Table 2)"***
- ***Line 284: added "The simulations reported in this work are specific to the Indian scenarios discussed."***
- ***Line 290: added "from a comparison of the correlation coefficients"***
- ***Line 315: changed "North" to "north"***
- ***Line 320: changed "more of the spatial distribution" to "more of the model spatial distribution than the observed slant columns"***
- ***Line 371: added "slant" before "columns"***
- ***Line 372: changed "those" to "observed distributions"***
- ***Line 375: removed "that"***
- ***Line 376: changed "of" to "from"***
- ***Line 379: Added sentence referring to Mahajan et al. (2015)***
- ***Line 396: changed "above" to a section reference***
- ***Line 409: re-wrote sentence regarding leaf thermotolerance***
- ***Line 413: added hyphen***
- ***Line 432: spelling correction***
- ***Line 452: changed "like" to "likely"***
- ***Line 457: spelling correction***
- ***Line 463: used order symbol***
- ***Line 470: changed "The transportation sector" to "Emissions from the transportation sector"***
- ***Line 471: changed "has peak" to "peak"***
- ***Line 477: changed "data collected using" to "data collected from"***
- ***Line 482: added "for the whole country"***
- ***Line 490: revised statement regarding further work***
- ***Line 503: changed "that correspond to MODIS land cover" to "with MODIS land cover"***

- ***Line 508: corrected citation format***
- ***Line 514: revised statement regarding linear relationship***
- ***Line 528: added sentence regarding Zhu et al 2016***
- ***Line 558: spelling correction***
- ***Line 559: changed "VOC" to "VOCs"***
- ***Line 563: moved "only" within this sentence***
- ***Line 566: changed "proposed an argument" to "argue"***
- ***Line 585: changed "Achieving this capability is greatly enhanced" to "Our ability to achieve this capability is improved"***
- ***Line 586: added "aboard Sentinel-5P"***
- ***Line 589: added Data availability section***
- ***Figure 1: Figure 1A replaced with clearer version and caption edited accordingly. Figure 1B slightly edited to give greater contrast. Header labels added to Figures 1B and 1C. Two grammar corrections in caption/***
- ***Figure 2: Units clarified as atom C/cm^2/s. Label added to 2C.***
- ***Figure 3: In caption, changed "per unit C" to "per-C"***
- ***Figure 4: Himalayas and Rann of Kutch highlighted***
- ***Figure 5: "Northeast", "East forest", "Kerala" labelled***
- ***Figure 7: Caption corrected***
- ***Figure 12: Underlying imagery changed, and caption accreditation changed accordingly***
- ***Table 1: Caption changed to indicate T, RH and BLH are from GEOS-Chem***
- ***Table 2: changed "per unit C" to "per-C"***
- ***Table 3: Units clarified as atom C/cm^2/s. % change from a priori column added***

4. Final manuscript with highlighted changes

The revised manuscript it appended to this document with changes highlighted. Removed text is shown in red, inserted text in blue.

Manuscript prepared for Atmos. Chem. Phys.
with version 2014/09/16 7.15 Copernicus papers of the LaTeX class copernicus.cls.
Date: 19 February 2018

Which processes drive observed variations of HCHO columns over India?

Luke Surl[1,2], Paul I. Palmer[1,2], and Gonzalo González Abad[3]

[1]National Centre for Earth Observation, University of Edinburgh, Edinburgh, UK.
[2]School of GeoSciences, University of Edinburgh, Edinburgh, UK.
[3]Atomic and Molecular Physics Division, Harvard–Smithsonian Center for Astrophysics, Cambridge, Massachusetts, USA

Correspondence to: Paul I. Palmer (paul.palmer@ed.ac.uk)

Abstract. We interpret HCHO column variations observed by the Ozone Monitoring Instrument (OMI), aboard the NASA Aura satellite, over India during 2014 using the GEOS-Chem atmospheric chemistry and transport model. We use a nested version of the model with a ~~spatial~~ horizontal resolution of approximately 25 km. HCHO columns are related to local emissions of volatile organic compounds (VOCs) with a spatial smearing that increases with the VOC lifetime. Over India, HCHO has biogenic, pyrogenic, and anthropogenic VOC sources. Using a 0-D photochemistry model, we find that isoprene has the largest molar yield of HCHO that is typically realized within a few hours. We find that forested regions that ~~neighbours~~ neighbour major urban conurbations are exposed to high levels of nitrogen oxides. This results in depleted hydroxyl radical concentrations and a delay in the production of HCHO from isoprene oxidation. We find that propene is the only anthropogenic VOC emitted in major Indian cities that produces HCHO at a comparable (but slower) rate to isoprene. The GEOS-Chem model reproduces the ~~broadscale~~ broad-scale annual mean HCHO column distribution observed by OMI (r=0.6), which is dominated by a distinctive meridional gradient in the northern half of the country, and by localized regions of high columns that coincide with forests. Major discrepancies are over the Indo-Gangetic Plain and Delhi. We find that the model has more skill at reproducing observations during winter (JF) and pre-monsoon (MAM) months with Pearson correlations r>0.5 but with a positive model bias of $\simeq 1\times10^{15}$ molec/cm^2. During the monsoon season (JJAS) we reproduce only a diffuse version of the observed meridional gradient (r=0.4). We find that on a continental scale most of the HCHO column seasonal cycle is explained by monthly variations in surface temperature (r=0.9), suggesting a role for biogenic VOCs, in agreement with the 0-D and GEOS-Chem model calculations. We also find that the seasonal cycle during 2014 is not significantly different from the ~~2008–2015~~ 2008–2015 mean seasonal variation~~but there are~~

~~large year to year variations~~. There are two main loci for biomass burning (states of Punjab and Haryana, and northeastern India), which we find ~~only~~ contributes a significant contribution (up to 1×10^{15} molec/cm^2) to observed HCHO columns ~~during March to~~ only during March and April over northeastern India. The slow production of HCHO from propene oxidation results in a smeared hotspot over Delhi that we resolve only on an annual mean timescale by using a temporal oversampling method. Using a linear regression model to relate GEOS-Chem isoprene emissions to HCHO columns we infer seasonal isoprene emissions over two key forest regions from the OMI HCHO column data. We find that the *a posteriori* emissions are typically lower than the *a priori* emissions, with a much stronger reduction of emissions during the monsoon season. We find that this reduction in emissions during monsoon months coincides with a large drop in satellite observations of leaf phenology that recovers in post monsoon months. This may signal a forest-scale response to monsoon conditions.

1 Introduction

Formaldehyde (HCHO) is an important source of the hydroperoxyl radical (Volkamer et al., 2010; Whalley et al., 2010), and a source of upper tropospheric hydroxyl radical (OH) (Jaeglé et al., 1998). It therefore plays a role in determining the oxidizing capacity of the global troposphere. The principal source of HCHO is from the oxidation of methane (CH_4), which provides a global ambient background. Shorter-lived non-methane volatile organic compounds (NMVOCs) elevate HCHO concentrations over continental atmospheres. Minor direct HCHO sources include biomass burning, industry, agriculture, automobiles, shipping, and vegetation. The atmospheric lifetime of HCHO, determined by OH and photolysis, is typically several hours. Building on our past studies (Palmer et al., 2003, 2006; Barkley et al., 2008; Gonzi et al., 2011), we interpret HCHO column distributions over India observed by the Ozone Monitoring Instrument (OMI) aboard the NASA Aura spacecraft (Levelt et al., 2006). We interpret spatial and temporal variations in terms of biogenic, pyrogenic, and anthropogenic VOC sources.

India has the sixth largest economy and the second largest population of any country. It also has one of the largest increases in mortality rates due to chronic exposure to elevated levels of surface ozone and particulate matter (Cohen et al., 2017). Figure 1 shows that India has a rich landscape that includes the Thar desert over northwestern India, major forests over the southwestern coast and over the east and northeast, and five megacities (New Delhi, Mumbai, Kolkata, Bengalura, and Chennai). The Indo-Gangetic Plain (IGP) stretches from eastern Pakistan, across the northern edge of India (bounded by the Himalayas), to Bangladesh. The IGP represents more than a quarter of a million acres of fertile land, which is used primarily to grow rice and wheat, but also maize, sugarcane, and cotton. The southwest monsoon represents the main source of water to the IGP, with contributions also from rivers flowing from the Himalayas. The southwest monsoon begins in June and subsides

in September. High temperatures over the Thar desert cause a region of low pressure that helps to establish a large-scale land-sea breeze with the Indian Ocean. This results in warm, moisture-laden air from the Indian Ocean travelling inland. Eventually, this air meets the Himalayas where it is forced to rise. As the air rises, cooler temperatures result in precipitation. Some areas of India receive ten metres of rain annually, mostly during the monsoon season.

Satellite columns observations of HCHO were originally developed using observed UV spectra from the Global Ozone Monitoring Experiment (Thomas et al., 1998; Chance et al., 2000). HCHO column data are now available from a range of satellite instruments, but here we focus on data from ~~the Ozone Monitoring Instrument~~ OMI aboard the NASA Aura spacecraft. Generally, slant HCHO columns are retrieved by directly fitting to observed spectra in a narrow UV window (Chance et al., 2000; De Smedt et al., 2008; González Abad et al., 2015). Vertical columns are determined by scaling these slant columns by scene-dependent air-mass factors (AMFs), taking into account clouds and aerosol scattering (Palmer et al., 2001). Past work has shown that HCHO columns over India have increased nationwide on average between 1.6%/yr (1997–2009, De Smedt et al. (2010)) and 1.5%/yr (1995-2013, Mahajan et al. (2015)). Mahajan et al. (2015) also showed using coincident satellite measurements of HCHO and NO_2 that over much of India O_3 production is limited by the availability by nitrogen oxides but over urban regions it is limited by the availability of VOCs, supported by detailed modelling studies over Delhi (Sharma et al., 2016). Here, we employ a high-resolution ($\simeq$25 km) model of atmospheric chemistry that is closely aligned with the resolution of the satellite data, allowing us to take advantage of the richness of these data.

HCHO columns are related to their parent VOC emissions with a smearing spatial scale that is related to the production rate and molar yield of HCHO (Palmer et al., 2003). Past studies have used this ~~approach~~ relationship to infer isoprene emissions from major forests ~~(Palmer et al., 2003; Abbot et al., 2003; Shim et al., 2005; P~~ biomass burning emissions (Young and Paton-Walsh, 2010; Gonzi et al., 2011; Stavrakou et al., 2016), and anthropogenic emissions (Fu et al., 2007; Stavrakou et al., 2009). Detailed photochemical calculations that link VOCs and the time-dependent production of HCHO lay the groundwork for interpreting the HCHO column data. Many past studies have inferred VOC emissions from the HCHO columns using a linear regression model between these two variables (e.g. Palmer et al. (2003); Millet et al. (2008)), but others have adopted a more rigorous Bayesian inverse model approach (e.g. Shim et al. (2005)). For central Africa, Marais et al. (2012) employed an inversion method that accounted for the NO_x dependence of the isoprene-HCHO relationship. Given the large uncertainties associated with VOC emissions (e.g. Guenther et al. (2012)) and the production of HCHO in the ~~low NO~~low-NO_x regime (Wolfe et al., 2016) both approaches provide useful insights. Our study is focused on India where there are significant sources of biogenic, pyrogenic, and anthropogenic VOCs.

The next section describes the OMI HCHO column data, the detailed box-model used to study the time-dependent production of HCHO from VOC oxidation, and the GEOS-Chem atmospheric

chemistry transport model focused on India. Section 3 reports the results from our analysis of the OMI HCHO column data over India, the associated model interpretation of these data, and the isoprene emissions we infer from the HCHO column data collected over two major forest regions. We conclude in Section 4.

2 Data and Methods

Our data are focused on India, as defined by the database of Global Administrative Areas (www.gadm.org). We adopt climatological definitions of seasons from the Indian Meteorological Department that are determined by the onset of the regional monsoon system: winter includes January and February; the pre-monsoon season is from March to May; the monsoon season is from June to September; and the post-monsoon season is from October to December. Our focus is on OMI HCHO column variations during 2014, but we put this year into a longer temporal context by comparing it with data collected from 2008 to 2015.

2.1 Ozone Monitoring Instrument HCHO Columns

For our analysis we use HCHO vertical columns from ~~Ozone Monitoring Instrument (OMI)~~OMI, a nadir-viewing UV/Vis spectrometer aboard the NASA Aura satellite that was launched in 2004. Aura is in a sun-synchronous orbit with a local equatorial crossing time of 13:38, achieving daily global coverage subject to cloud coverage.

OMI uses two imaging grating spectrometers each with a CCD detector to collect solar backscattered radiation in the spectral range 270–500 nm using three channels: UV-1 (264–311 nm), UV-2 (307–383 nm), and Vis (349–504 nm). OMI has an across-track swath width of 2,600 km, which in global mode is described by 60 scenes that have ground footprints from 13×24 km^2 at nadir to 28×160 km^2 at the swath edges.

Determination of HCHO vertical columns is a two-step procedure, which we describe below. First, slant columns are retrieved from the observed spectra. Second, an air-mass factor (AMF) is used to transform these slant columns into geophysical vertical columns that can be compared more easily with models.

We use the NASA OMHCHOv003 data product (González Abad et al., 2015) from the NASA Data and Information Services Center, which fits HCHO slant columns in the 328.5–356.5 nm window and accounts for competing absorbers, the Ring effect, and undersampling. Typical slant columns range from 4×10^{15} to 6×10^{16} molec/cm^2 with associated fitting uncertainties ranging from 30% for larger columns to more than 100% for smaller columns (González Abad et al., 2015).

We adopt a conservative approach to filtering data, based on previous studies (e.g. De Smedt et al. (2015)). We filter slant column data using the main data quality flag (removing suspect, bad or missing scenes); scenes that have been flagged as being affected by the row anomaly corresponding

to problem with a row of CCD detectors on OMI; scenes with slant column values greater than 15×10^{16} molec/cm^2 that we attribute also to potential row anomalies; scenes with solar zenith angles less than 0° or greater than 70°; scenes with cloud fractions > 0.4; and scenes from the last two rows at the edge of the swath, which we are too wide to be useful in our analysis. We do not anticipate that these data filters will introduce bias in our anlysis, with the exception of removing cloudy scenes that introduces a clear-sky bias. To evaluate the clear-sky bias, we compared the corresponding model HCHO columns (described below) with and without these cloudy scenes and find that removing them results in a monthly mean positive bias of 13%, consistent with previous work (Palmer et al., 2001).

To transform each observed slant column to a vertical column we calculate an AMF that accounts for temporal and spatial variations from scattering due to clouds and aerosols, and for the vertical distribution of HCHO. This approach is described in ~~detailed~~ detail by Palmer et al. (2001); Martin et al. (2003), and has since been evaluated in a large number of studies (e.g., Palmer et al. (2003, 2006); Fu et al. (2007); Millet et al. (2008); Barkley et al. (2008); Curci et al. (2010); Gonzi et al. (2011); Marais et al. (2012)). We use the OMI OMCL02 cloud data product, and the nested GEOS-Chem model to provide information about aerosols and HCHO vertical distributions, described below.

Finally, as a post-processing step, we remove any large-scale biases using a reference sector normalization procedure (Palmer et al., 2003; Martin et al., 2003). Over the remote Pacific we expect observed HCHO columns to be determined exclusively by the oxidation of methane. By anchoring observed values over the remote Pacific (0–40°N, 160–180°W) to the corresponding GEOS-Chem model values we determine the monthly bias that we subsequently subtract from the data within the study domain.

Previous work using aircraft observations over Southeastern U.S. has reported that the OMHCHOv0003 OMI HCHO column data product has a negative bias (37%), and that the GEOS-Chem model (v9-02) has a 10% negative bias (Zhu et al., 2016). In the absence of similar data over India, we cannot determine with certainty the generality of these biases, and have chosen to implicitly assume that the OMI data are not significantly impacted by systematic error

2.2 Models of Tropospheric Chemistry

We use the CAABA box model, including a comprehensive description of atmospheric chemistry, to understand the time-dependent yield of HCHO from the oxidation of VOCs in Indian forest and urban environments. These calculations help determine which VOC emissions are responsible for observed HCHO column variations. We also use a nested version of the GEOS-Chem 3-D atmospheric chemistry model to interpret the satellite data and to understand chemistry on a regional spatial scale. We use this model to establish a relationship between emissions of VOCs and HCHO columns that is used to infer emissions of VOCs that correspond to observed HCHO columns.

The chemical mechanisms from the CAABA box model and the GEOS-Chem model are not identical. CAABA includes a more explicit chemical mechanism and a reduced version of the Mainz Isoprene Mechanism 2 (MIM2, Taraborrelli et al. (2009)). The version of GEOS-Chem we use here is described by Eastham et al. (2014). The latest version of the GEOS-Chem chemical mechanism, released after the majority of our calculations had been completed, results in an increase of the HCHO yield from the oxidation of isoprene. We find using preliminary calculations with v11-01 that the revised mechanism does not systematically change the results shown here. Previous studies have evaluated the performance of GEOS-Chem (Marvin et al., 2017) and MIM2 (Taraborrelli et al., 2009) against the Master Chemical Mechanism. The GEOS-Chem v10-01 mechanism slightly underestimates HCHO production in high-NO_x conditions and the MIM2 mechanism shows similar HCHO production across a wide range of NO_x values.

Box modelling

We use v3.0 of the CAABA/MECCA (0-D) box model (Sander et al., 2011), but without halogen, sulphur, and mercury chemistry, to estimate the time-dependent production of HCHO from the chemical oxidation of different VOCs in forest and urban photochemical environments (Table 1).

We set up the model to describe a well-mixed summertime boundary layer, with photochemistry driven by a diurnal cycle in sunlight. For each environment, the photolysis model JVAL ~~Sander et al. (2014)~~ (Sander et al., 2014) is used to calculate photolysis rates assuming clear-sky conditions given latitude, longitude, and day of year. For each study location, we assume constant values for humidity, pressure, temperature and boundary layer height, taken from colocated GEOS-FP meteorology (see below). For forested environments we also prescribe fixed mixing ratios of O_3, NO_2 and CO from the GEOS-Chem model, described below. For the Delhi urban environment we use daytime average surface air pollutant values in 2014 reported by Tyagi et al. (2016): O_3 (37 ppbv), CO (2.3 ppmv), and NO_2 (19 ppbv), Table 1. Figure 1 shows the three forested regions (denoted by E, NE, and S) we chose to explore the range of photochemical environments. For each calculation, we spun-up the model from initial conditions for 48 hours before running the model for a further seven days. We use a model timestep of two minutes.

To evaluate the time-dependent HCHO yield of anthropogenic and biogenic VOCs we run paired calculations: 1) a control run and 2) a run in which we perturb a VOC by approximately 5×10^{14} molec cm^{-2} over a 15 minute period at 0900 local time on the first day after the two-day spin-up period. The perturbed amount is sufficiently small that we can assume that the chemistry response is approximately linear so that we can compare the perturbed run with the control run. We can then use control minus perturbed model calculations to determine HCHO per-carbon yield from the oxidation of the perturbed VOC.

GEOS-Chem 3-D Modelling

We use v10-01 of the GEOS-Chem global model of atmospheric chemistry and transport (www.geos-chem.org), driven by GEOS-FP analyzed meteorological fields, provided by the Global Modeling and Assimilation Office (GMAO) at NASA Goddard Space Flight Center. The native spatial resolution of these data is $0.25°$ (latitude) $\times 0.3125°$ (longitude), and includes 47 vertical terrain-following ~~signal-levels~~ sigma-levels that describe the atmosphere from the surface to 0.01 hPa of which about 30 are ~~in the troposphere~~typically below the dynamic tropopause. The 3-D meteorological data are updated hourly, and 2-D fields and surface fields are updated every 3 hours. The chemical mechanism used is the "tropchem" mechanism (Eastham et al., 2014). The atmospheric chemistry and transport timesteps are five and ten minutes, respectively.

We use the nesting capability of the model to focus on India, defined here as 0–40°N, 65–100°E, using the native resolution of the meteorological data. We use time-dependent lateral boundary conditions archived from a self-consistent, $4° \times 5°$ version of the global full-chemistry model, which is initialized in January 2013 to minimize the influence of initial conditions. Here, we describe emission inventories relevant to our nested India simulation and direct the reader to the GEOS-Chem website (http://geos-chem.org) for a more comprehensive description of inventories.

Monthly anthropogenic emissions for India are taken from the mosaic MIX inventory (Li et al., 2017), including NO, CO, SO_2 and NMVOCs that are available on a spatial resolution of ~~of~~ $0.25 \times 0.25°$. The emissions for India are a mosaic of regional emission inventories, including the Regional Emission inventory in ASia (REAS) (Kurokawa et al., 2013) and those developed by the Argonne National Laboratory (Lu et al., 2011; Lu and Streets, 2012). Indian NMVOC emissions represent by mass 17 Tg per year, of which 43% is from the residential sector, 36% is from transport, 20% is from industry, and a small amount is attributed to the power sector.

Approximately 20% of India's geographical area is described as forest. To describe biogenic VOC emissions of isoprene, monoterpenes, alkenes, and acetone we use the MEGAN v2.1 emission model (Model of Emissions of Gases and Aerosols from Nature, Guenther et al. (2012)). Figure 2 shows seasonal isoprene emissions over India. Monoterpenes emission have a similar distribution to isoprene but are a factor of five smaller in magnitude. Given their relatively small influence on HCHO column variability (Palmer et al., 2003) we do not discuss them further. Within GEOS-Chem, we adjust the MEGAN model with time-dependent local environment conditions (e.g., surface temperature, photosynthetic active radiation, and leaf area index ~~, LAI)~~ (LAI) from MODIS).

Monthly pyrogenic emissions are taken from the Global Fire Emissions Database (GFED) version 4 (van der Werf et al., 2017), which are available with a spatial resolution of $0.25 \times 0.25°$. ~~For a comprehensive description of the emissions inventories used by GEOS-Chem the reader is referred to the GEOS-Chem website ().~~

To interpret OMI HCHO column data we sample the model at the local time averaged between 1300 and 1500, corresponding to the overpass time of OMI, and the location of each observed

scene. To put 2014 into a broader temporal context, we interpreted OMI HCHO columns for years 2008–2015. ~~Due to computational limitations, we used the 2014 model run for the other years, ignoring year-to-year changes in atmospheric transport.~~ We find that the AMF plays only a minor role in determining OMI vertical column variations so we do not expect our approach to significantly influence our study of year to changes in the HCHO columns.

3 Results

First, we report results from the box-model calculation to provide some insights into the VOCs that determine the observed HCHO column variations. We then report the annual and seasonal spatial distributions of OMI and GEOS-Chem HCHO columns. Using correlative space-borne data we explore the role of biogenic, pyrogenic, and anthropogenic emissions in determining the spatial distributions of HCHO. Finally, using a model relationship between isoprene emissions and HCHO columns we infer isoprene emissions that are consistent with the OMI vertical columns.

3.1 HCHO Yield from VOC Oxidation in Urban and Forest Environments

We use the CAABA/MECCA box model to determine the time-dependent production of HCHO from the VOCs that we expect to be emitted from urban and forest environments over India. This represents important groundwork for interpreting the satellite observations of HCHO. Table 1 provides an overview of the box model calculations we describe below.

Relating HCHO column variations to emissions of its parent VOC requires that the VOC 1) has a high yield of HCHO so that eventual concentrations are elevated above the global background, determined mainly by the oxidation of CH_4; and 2) produces HCHO rapidly so that most of the HCHO is produced close to the emission source and not smeared over long spatial scales. Isoprene is the dominant HCHO precursor over many northern midlatitude and tropical forest ecosystems (Palmer et al., 2003, 2006; Barkley et al., 2008; Curci et al., 2010). Over tropical latitudes biomass burning emissions of VOCs also play a role in HCHO column variations (Fu et al., 2007; Barkley et al., 2008; Gonzi et al., 2011; Marais et al., 2012). Fu et al. (2007) also showed that reactive anthropogenic VOCs played a role in HCHO column variations over China.

Biogenic VOCs from Forest Environments

We explore three contrasting forest regions throughout 2014 (Figure 1), characterized by latitude-dependent levels of photosynthetically active radiation (PAR) and by their proximity to urban emissions. We focus on the yield of HCHO from the emission of isoprene (Palmer et al., 2003).

For each calculation we report in Table 2 the resulting lifetime of the injected isoprene (section 2.2), and the cumulative ~~per C~~ per-C HCHO yield. We find that the duration of the calculation is sufficiently long that the peak HCHO had time to diminish to a negligible amount.

The atmospheric lifetime of isoprene against OH is typically much shorter than an hour, with shortest values (<15 mins) during summer months. The most southern site in the state of Kerala (Figure 1) is where isoprene has the longest lifetime. This is due to OH being suppressed by high ambient NO_2 concentrations (in excess of 8 ppbv) originating from the coastal conurbation in that state. We find that levels of NO_x are sufficiently high (~~>~~averages generally around or above 1 ppbv) in all forested regions such that isoprene peroxy radicals preferentially react with NO to rapidly produce HCHO. Peak values for HCHO production are typically reached within 90 minutes of the isoprene ~~getting oxidized~~oxidation. The OH suppression in Kerala is primarily responsible for the slow production of HCHO. We find that the peak HCHO signal is typically reached within 30-90 minutes, corresponding to a smearing length scale of 9–27 km assuming an example wind speed of 5 m/s. For the Kerala region where the time taken to reach the peak HCHO signal is typically 2–3 hours the corresponding smearing length scale is 36–54 km. Even in Kerala the smearing length is comparable to the longitudinal extent of a single OMI scene and well within the swath width (section 2). Figure 3 shows that the corresponding values of the per-C HCHO yield ranges from 0.38 to 0.66. Higher values are generally associated with higher values of NO_x (c.f. NO_2 mixing ratios in Table 1 and yields reported in Table 2), consistent with previous studies (Palmer et al., 2006; Barkley et al., 2013). The simulations reported in this work are specific to the Indian scenarios discussed.

Anthropogenic VOC in urban environment

To study the role of anthropogenic non-methane VOCs (NMVOCs) in determining HCHO columns we simulate boundary layer chemistry over Delhi using emissions from the MIX emission inventory (Li et al., 2017). Over major cities, NMVOC emissions originate mainly from stationary combustion and the transport sector. The species in the MIX inventory are defined following the SAPRC-99 chemical mechanism (Carter, 2000). ~~We~~ From a comparison of the correlation coefficients we find that over Delhi, according to the MIX inventory, NMVOC emissions include propane, propene and ALK4, representing 13%, 32%, and 55% of NMVOC C emissions. ALK4 denotes $>C_4$ alkanes. The longest chain alkane in the 0-D chemical mechanism is n-butane. We denote this urban model scenario as "D05" (Table 1). We calculate individual HCHO yields from the oxidation of propane, propene, and n-butane.

Propene ($CH_3CH{=}CH_2$) has an atmospheric lifetime of several hours, determined by OH addition to its double bond. The major intermediate products include HCHO and acetaldehyde. The ultimate HCHO yield from the oxidation of propene (close to 0.5) is comparable with the value from isoprene oxidation (Figure 3) but it only reaches 50% of that final value within 12 hours, consistent with the longer lifetime of propene. Propane and n-butane have atmospheric lifetimes of 10 and 5 days, respectively, determined by OH. Long-lived intermediate oxidation products include acetone that further delay the production of HCHO (Figure 3).

Assuming an average wind speed of 3 m/s, taken from wind measurements at Indira Ghandi airport in Delhi, only HCHO production from the oxidation of propene (out of all the gases that represent a major contribution to the regional emission inventory) would produce a signal that could potentially be distinguishable above the ambient concentration. We show later there is some evidence that we can observe a Delhi HCHO hotspot but only after temporally oversampling the data.

3.2 OMI and GEOS-Chem Model HCHO Column Distributions

Data Filtering and AMF Statistics

Using the data quality criteria, as defined above, we remove 58% of all OMI HCHO measurements collected during 2014. The proportion of data removed per month varies during the year, with most scenes removed during the cloudy monsoon season in July (71%) and the least number of scenes removed during March (45%).

Figure 4 shows the annual mean distribution of AMFs across India. AMF values range from 0.7 to 1.5 with a median value of 1. AMF values are highest in the Himalayas at the extreme ~~North~~ north of India, which are often covered by snow, and over the Rann of Kutch salt marsh. In both cases, elevated AMF values are due to high surface albedos.

To determine the influence of the AMFs on the spatial distribution of HCHO vertical columns we compare fitted OMI slant HCHO columns and the corresponding vertical columns to the GEOS-Chem model. We find that the vertical columns reproduce 11% more of the ~~spatial distribution~~model spatial distribution than the observed slant columns, consistent with past studies (Palmer et al., 2001; Millet et al., 2008) that show that the AMF plays only a minor role in the observed spatial distribution of vertical HCHO columns.

To investigate the role of model resolution in our calculation of vertical columns we repeated the annual mean analysis using the $2^\circ \times 2.5^\circ$ version of the GEOS-Chem driven by the same inventories as described above. Figure 5 shows that the coarser resolution model fails to reproduce smaller-scale variations, as expected, that define much of the India western coast, and misses variations over northeastern India. While the model via the AMF calculation only contributes a small amount to the distribution of HCHO vertical columns it does affect the magnitude of the columns. We find that there is an overwhelming argument to justify the use of the higher-resolution model.

Annual Mean Spatial Distribution

Figure 5 shows the annual mean model and observed HCHO columns for 2014. The lowest observed and model columns are in the north of the study region coinciding with the Himalayas and (to a lesser extent) in the Thar desert in the Northwest. The observations show three main regions associated with elevated HCHO columns: 1) the non-Himalayan part of the Northeast region of India, east of Bangladesh; 2) territory at the south of the country, around the southern part of the Western Ghats

mountain range, roughly following the borders of the state of Kerala; and 3) a broad area over the east of the country, roughly outlined by the states of Chattisgarh, Odisha, and the northern part of Anhdra Pradesh.

The nested GEOS-Chem model reproduces the observed magnitude and broad-scale spatial distribution of OMI HCHO columns over India (Figure 5), but is much smoother. The model has a small but positive bias of 14% (12%) for the mean (median) annual column amounts. We find that the model captures 33% (r=0.58) of the observed annual mean spatial variation of HCHO columns. The major discrepancy between the model and observed annual mean HCHO distributions is over the IGP and over Delhi. Observed HCHO columns are elevated over the IGP but not to the values shown in the model, which we discuss below. A HCHO hotspot over Delhi is apparently absent from the OMI columns, but as we show later there is evidence that the hotspot exists in the observations.

Based on the box modelling, the largest source of HCHO column variability is expected to be isoprene emissions. Figure 1 shows that the broad-scale annual distribution of HCHO over India is consistent with the annual mean distribution of Normalized Diffusive Vegetation Index (NDVI) with a Pearson correlation of r = 0.49. Below, we use seasonal variations of HCHO columns to improve understanding of the drivers.

3.3 Seasonal Spatial Distributions

Figure 6 shows OMI and GEOS-Chem model HCHO columns for seasons during 2014. There are distinct seasonal cycles to the HCHO columns over three broad regions: northeastern and southwestern India, and over the IGP. Over (north)eastern India HCHO columns peak in pre-monsoon and monsoon months. Columns over southwestern coast of India peak in winter and pre-monsoon months and are very low in other seasons. Columns over the IGP are elevated above those elsewhere in northern Indian during pre-monsoon months and peak in monsoon months. Figure 7 shows that the timing of these elevated columns coincide with warmer surface temperatures. This suggests a role for biogenic VOC emissions, consistent with the strong, local relationship between isoprene emissions and HCHO production that we demonstrated above.

The GEOS-Chem model captures these broad-scale observed distributions of HCHO but is much smoother, as expected. We find the model has some skill at reproducing the observed spatial distribution with a Pearson correlation r of $>$0.4, with larger values in winter and pre-monsoon months (r=0.50 and 0.62, respectively) and smaller values in monsoon and post-monsoon months (r=0.39 and 0.44, respectively). On an annual timescale the model has a positive bias of 1.0×10^{15}molec/cm^2 (33%), which is skewed due to a large bias during the monsoon months (1.9×10^{15}molec/cm^2, 17%). The model has a more defined peak over Delhi, peaking in monsoon months, but there is only a small, diffuse peak in the observations. We discuss this discrepency below.

Figure 7 shows that on a continental scale the seasonal distribution of HCHO slant columns over India in 2014 is not significantly different from ~~those~~ observed distributions from 2008 to 2015. In

general, HCHO columns follow a similar cycle in the winter and pre-monsoon months, but there are substantial year to year variations during the monsoon and post-monsoon months suggesting a role for large-scale variation in meteorology associated with the monsoon. Figure 8 shows ~~that~~ the corresponding differences in the spatial distribution of HCHO columns ~~of~~ from 2014 compared to the mean 2008–2015 distribution. Median HCHO columns for 2014 are slightly higher than the eight-year average by 0.4×10^{15}molec/cm^2, but show a similar spatial distribution taking into account ~~year to year~~ year-to-year variability (Figure 7). Mahajan et al. (2015) reports an analysis of the drivers of year-to-year variations in HCHO columns over India.

Biogenic VOCs

Figure 7 shows that the observed continental-scale HCHO seasonal cycle is reproduced by the model but with a positive model bias typically within 1×10^{15} molec/cm^2. On this spatial scale, most of the seasonal cycle can be explained by variations in surface temperature, suggesting a larger than expected role for biogenic emissions. However, the model fails to capture the elevated monthly column during October 2014. We find this is driven mostly by observed variations in HCHO columns over tropical India, coinciding with the withdrawal of the monsoon from India between late September and mid-October (Pai and Bhan, 2015). We suggest this variation represents a response from the vegetation that is missing in the model. Model error associated with cloud coverage and consequent errors associated with the partioning between direct and diffuse PAR could result in large-scale changes in biogenic emissions.

The only forested region that is the exception to the continental-scale picture is over Kerala (denoted by S in Figure 1). Kerala has a tropical maritime climate with little seasonal variation in temperature. The forested region in Kerala neighbours an urban conurbation associated with a high level of NO_x (Figure 9), which influence the HCHO yields from the oxidation of biogenic VOCs, as described ~~above~~in Section 3.1. Figure 10 shows that the observed seasonal distribution of HCHO columns at this site, broadly reproduced by the model, peaks during the winter and is lowest during pre-monsoon and monsoon months. The size of the seasonal variation in HCHO columns is not fully explained by the small seasonal variation in surface temperature, suggesting a role for an additional driver. Figure 10 shows that over this region, the seasonal distribution is driven mostly by changes in leaf phenology rather than temperature or PAR. Satellite observations of LAI drop from $\simeq$4 m^2/m^2 to $\simeq$1 m^2/m^2 during the monsoon months and recover in the post-monsoon months. We find similar behaviour over the east and northeastern forests with large reductions in LAI during monsoon months (not shown). This behaviour is consistent with vegetation taking advantage of the decreased temperatures and higher precipitation rates during the monsoon season to regulate leaf flushing.

Past work has found a contrasting relationship between leaf phenology and satellite observations of HCHO columns over the Amazon basin (Barkley et al., 2009) in which HCHO columns and LAI values dropped in the transition period between the wet and dry seasons, and recovered

soon afterwards. ~~Leaves produce isoprene as a thermotolerance mechanism (Singaas et al., 1997), with new leaves having a higher capacity to produce isoprene that deteriorates~~ Thermotolerance is one hypothesis that describes why leaves emit isoprene (Singaas et al., 1997). After a few weeks of emerging, the emission capacity of leaves peaks and subsequently declines with age. To explain the variation in HCHO columns, Barkley et al. (2009) proposed ~~widescale~~ wide-scale leaf flushing that allowed vegetation to maximize their protection against the light-rich environment of the dry season. A demographic model of leaf phenology based on the hypothesis that trees seek an optimal LAI as a function of available light and soil water (Caldararu et al., 2012, 2014) explained the observed increase in LAI over the Amazon basin during the dry season as a net addition of leaves in response to increased solar radiation.

Pyrogenic VOCs

The main loci for biomass burning are: 1) a region approximately encompassed by the state boundaries of Punjab and Haryana (Figure 1) and 2) Northeastern India. The states of Punjab and Haryana have two growing seasons: May–September (rice) and November–April (wheat). Paddy stubble burning in May and October/November represents agriculture burning of wheat and rice residue, respectively. For our purposes Northeastern India includes the Seven Sister states (Arunachal Pradesh, Assam, Meghalaya, Manipur, Mizoram, Nagaland, and Tripura), where there are significant forest fires particularly during March and April. This is mainly due to deforestation to convert forests to agricultural land (Santenda and Kaushik, 2014). These two geographical regions account for more than 70% of these emissions during 2014.

To illustrate the impact of fires on HCHO column variations we use MODIS firecount data (Justice et al., 2002) to identify when and where fires occur over the states of Punjab and Haryana, and Northeastern India. We calculate monthly mean HCHO vertical columns and firecounts. We then determine which $0.25^\circ \times 0.3125^\circ$grid cells are most affected by fires by selecting ~~thes~~ these cells in the top 20th percentile of cumulative fires.

Figure 11 shows that the highest number of firecounts generally correspond to when there is the largest difference between all grid cells and those most affected by fire. This difference is relatively small over the states of Punjab and Haryana with a peak value of 1.5×10^{15} molec/cm^2 during May. There is a large difference during March and April over the Northeastern India where fires contribute up to 5×10^{15} molec/cm^2 to the monthly mean. We find that this contribution to HCHO columns is localized in time and geography.

Anthropogenic Hotspots

Guided by *a priori* emissions and our box modelling, we anticipate that propene is the only anthropogenic VOC likely to produce HCHO sufficiently rapidly that we can relate elevated HCHO columns to emissions. However, we find little evidence that seasonally-averaged OMI HCHO columns

are elevated over Indian megacities due to limits in the signal to noise, in agreement with previous work (Mahajan et al., 2015).

We use a temporal oversampling approach, following Zhu et al. (2014), to improve the spatial resolution of HCHO columns over Delhi and the surrounding region. Oversampling increases the signal-to-noise ratio and allows for inspection of finer spatial features, at the expense of the temporal information. We focus on Delhi because the National Capital Region has a population of approximately 17 million people (Perianayagam and Goli, 2012) over a geographical area of approximately 2000 km^2. Based on the MIX emissions inventory, which is indicative of values from 2010, (Figure 6) we expect to see an elevated signal from this region. This bottom-up emission inventory ~~like~~ likely overestimates emissions from the transport sector, which has seen the biggest change from 2010 to 2014 (per. comm.: Jun-ichi Kurokawa, Japan Environmental Sanitation Center, October 2017).

First, our area of focus is divided into a very high resolution grid ($0.02° \times 0.02°$). The temporally-averaged column for each point in this grid is the average of the OMI observational vertical columns ~~colected~~ collected during 2014 with the centre point within 43 km in both the latitudinal and longitudinal directions. This effectively smears out these observations over 43 km squares. Here, we average over 43×43 km^2 squares rather than the 24 km radius circles), sampling all the 2014 vertical HCHO columns from the observational dataset for the area around Delhi.

Figure 12 shows that the oversampling method results in distinct elevated HCHO columns over New Delhi and along major roadways, although the gradients are still noisy. The magnitude of this elevation is ~~a $\simeq 10^{15}$~~ $\mathcal{O}(10^{15})$ molec/cm^2. Elevated areas to the East and Southeast of the city may represent HCHO produced from VOC transported downwind from Delhi. Based on our results we find that anthropogenic emissions do not appear to play a large role in the observed column variations of HCHO over India.

However, our use of HCHO columns from the OMI instrument, which has a local overpass time of 1330, may be hindering our ability to observe the anthropogenic contribution to HCHO. Biogenic emissions and to a lesser extent biomass burning emissions peak in early afternoon hours, which is ideal for OMI. ~~The~~ Emissions from the transportation sector, a major source of anthropogenic VOCs, ~~has peaks~~ peak during early morning and late afternoon associated with commuter traffic. We argue that the early morning 0930 overpass of the Global Ozone Monitoring Experiment (GOME-2) aboard the MetOp satellite is better suited to capture these anthropogenic emissions. Secondary production of HCHO is generally larger than direct emissions of HCHO, and will occur a few hours after the peak commuter time (e.g. Lin et al. (2012); Wang et al. (2017)). The early morning rush hour in Delhi starts after 0700 so we expect a 0930 overpass to also capture some fraction of the secondary HCHO production. Using data collected ~~using~~ from morning and afternoon overpass times to describe diurnal variations of HCHO was presented by De Smedt et al. (2015), but they did not discuss the relative importance of different VOC emission sources at these different times.

Figure 13 shows the annual mean HCHO columns observed by GOME-2 and OMI. For our preliminary argument we are interested only in the distribution of HCHO columns. Here, we have standardized these data ~~so that that~~ for the whole country so that they have a mean of zero and a unit standard deviation using:

$$z_i = \frac{x_i - \bar{x}}{s}, \tag{1}$$

where x_i is a data point, $\bar{x}$ is the sample mean, and s is the sample standard deviation. This allows us to compare the two data without worrying about bias. The resulting z-scores represent the number of standard deviations from the population mean. We find that GOME-2 data has higher columns over the IGP, while OMI more clearly emphasizes the forested regions that we can identify independently through LAI or NDVI measurements (Figure 1). This qualitative test appears to support our hypothesis ~~but needs further work outside the scope of this current study.~~ and is an early demonstration of how datasets with continuous measurements of a region (such as those from a geostationary satellite) could help capture the temporal variability of HCHO. Taking advantage of the complementary information from multiple sensors that have different local overpass time requires a sophisticated inverse model approach.

3.4 Inferring Isoprene Emissions from OMI HCHO Columns

Based on our analysis of the HCHO yields from Indian VOC sources, and the distribution of observed HCHO columns we conclude that the majority of the observed HCHO column variation is due to biogenic VOC emissions. Here, we adopt a simple inversion methodology based on linear regression to infer isoprene emissions from OMI HCHO columns (Palmer et al., 2006).

First, we filter HCHO column data over India to minimize any interference from pyrogenic and anthropogenic sources. We focus on two relatively remote areas of India: "East" defined approximately as the area spanning 16–25°N and 76–87~~,~~°E, and "Northeast" defined as the region of India east of 90°E (Figure 1). We remove scenes ~~that correspond to~~ with MODIS land cover classifications (Friedl et al., 2010) corresponding to croplands (including cropland mosaics), urban/built-up, snow/ice, barren/sparsely vegetated, and water bodies. We also filter out potential fire-affected data by identifying for each day the cells of the $0.25° \times 0.3125°$grid in which fires are reported in the MODIS active fire product. The data from these, and the adjacent cells, are then removed for that day as well as the preceding and succeeding days, following ~~(Barkley et al., 2013)~~Barkley et al. (2013).

Second, we determine the model relationship between local isoprene emissions E (molec/cm^2/s), as calculated by MEGAN (Guenther et al., 2012), and HCHO columns Ω (molec/cm^2):

$$\Omega = SE_{\mathrm{VOC}} + \Omega_b, \tag{2}$$

where the slope S represents the production of HCHO column per emission of isoprene, and the intercept Ω_b represent the HCHO column contributions from longer-lived VOCs mainly from the

oxidation of methane. ~~To estimate isoprene emissions that are consistent with the HCHO columns we transpose this linear relationship .~~ We resolve seasonal *a priori* emissions of isoprene from observed HCHO columns by transposing the model linear relationship between isoprene emissions and HCHO columns.

For both study regions, we find a statistically significant linear relationship between those variables (Table 3), where Pearson correlation coefficients r range from 0.52 to 0.82, with a typical value in excess of 0.70. The slope values (10^3s) vary with region and season. The offsets that represent the background HCHO column is higher during the pre-monsoon and monsoon summer months when we expect larger HCHO production from a range of longer-lived VOC (including CH_4) due to higher values of OH.

Our *a posteriori* emission estimates are generally lower than *a priori* values, reflecting the positive model HCHO column bias. This is most pronounced over the Northeast during the monsoon season, where *a posteriori* isoprene emissions are 88% lower than *a priori* estimate, due to the model not capturing the sharp observed decline in HCHO that appears to be linked with monsoon conditions. We acknowledge that the bias between model and OMI HCHO columns could also reflect a bias in the OMI data (Zhu et al., 2016) but without independent measurements over this region we have chosen to assign these biases exclusively to the model.

4 Concluding Remarks

We used models of atmospheric chemistry to interpret HCHO column distributions during 2014 observed by the Ozone Monitoring Instrument (OMI) satellite instrument over India. The annual mean OMI distribution of clear-sky HCHO columns is dominated by a distinctive meridional gradient in the northern half of the country, and by localized regions of high columns that coincide with forests. We found that the nested GEOS-Chem atmospheric chemistry model (spatially resolved at $\simeq$25 km) reproduces these broad-scale observed features with a positive model bias, particularly over the Indo-Gangetic Plain and Delhi.

Over India, HCHO has biogenic, pyrogenic, and anthropogenic sources of volatile organic compounds (VOCs), some of which are spatially and temporally disaggregated. Using the CAABA 0-D photochemistry model, we explored a range of forest and urban photochemical environments found over India and their subsequent influence on HCHO concentrations. HCHO columns are related to local VOC emissions with a spatial smearing that increase with the VOC lifetime. We found that isoprene has the largest molar yield of HCHO that is typically realized within a few hours in the presence of moderate levels of nitrogen oxides ($\simeq$1 ppbv), in agreement with previous studies. However, we also found that forested regions that neighbour major urban conurbations (e.g. in the state of Kerala) are exposed to much higher levels of nitrogen oxides ($\simeq$8 ppbv). This results in depleted hydroxyl radical concentrations and a delay in the production of HCHO from isoprene oxidation.

Informed by a regional bottom-up emission inventory for India, we found that propene is the only major component of anthropogenic VOCs that produces HCHO at comparable (but slower) rate to isoprene.

We found that the GEOS-Chem model reproduces observed spatial distributions during winter (JF) and pre-monsoon months (MAM) better than during monsoon (JJAS) and post-monsoon (OND) months. We attributed these differences in model skill to the response of the natural biosphere to changes in the meteorological and photochemical environments associated with the onset and retreat of the monsoon. We found that on a continental scale much of the seasonal cycle in observed HCHO columns can be explained by monthly variations in surface temperature. This observation together with the strong local relationship we found between isoprene ~~nemissions~~ emissions and HCHO production suggests a role for biogenic ~~VOC~~VOCs, in agreement with the GEOS-Chem model calculation. We also found that the seasonal cycle during 2014 is not significantly different from the 2008-2015 mean seasonal variation but there are large year to year variations. There are two main loci for biomass burning (states of Punjab and Haryana, and northeastern India), which we found ~~only~~ contributes a significant contribution to observed columns only during March to April over northeastern India. The slow production of HCHO from propene oxidation results in a smeared hotspot over Delhi that we resolved only by using a temporal oversampling method. Based on comparing GOME-2 and OMI HCHO column distributions, we ~~proposed an argument~~ argue that the early morning overpass time is better for quantifying anthropogenic emissions soon after the rush hour and before biogenic emissions are at their early afternoon peak.

Using a linear regression model to relate GEOS-Chem isoprene emissions to HCHO columns we inferred seasonal isoprene emissions over two key forest regions from the OMI HCHO column data. We found that the *a posteriori* emissions are typically lower than the *a priori* emissions, with a much stronger reduction of emissions during the monsoon season. This reduction in emissions during monsoon months coincided with a large drop in satellite observations of leaf phenology. Large-scale differences in observed and model HCHO columns during monsoon months may highlight errors in seasonal variations in basal emission rates and/or model errors associated with the underlying meteorological environments, e.g. partitioning of direct and diffuse photosynthetically active radiation.

The next logical step to this analysis is to estimate simultaneous estimates of anthropogenic, pyrogenic, and biogenic VOC emissions by using data collecting data from morning and afternoon local overpass times. In the case of biogenic VOC emissions, information from HCHO columns together with leaf phenology (e.g. leaf area index) and land surface parameters (e.g., soil moisture), can be integrated to develop a new satellite data-driven isoprene emission inventory. A self-consistent pan-tropical emission inventory for isoprene, for example, would help to improve understanding of tropospheric O_3 and organic aerosol that represent some of the largest uncertainties associated with the Earth system. ~~Achieving~~ Our ability to achieve this capability is ~~greatly enhanced~~ improved by

the launch of TROPOMI aboard Sentinel-5P that will result in daily maps of HCHO columns and complementary trace gases at a spatial resolution of 7 km, which dramatically increases the number of clear-sky scenes available for the analysis.

5 Data availability

The OMHCHOv003 OMI HCHO column data are publicly available through NASA's Mirador website. Model data are achived at the Edinburgh Data Share http://dx.doi.org/10.7488/ds/2305.

Acknowledgements. L.S. was funded by the NERC National Centre for Earth Observation (NCEO020005), and P.I.P. gratefully acknowledges his Royal Society Wolfson Research Merit Award. L.S. also acknowledges funding from the British Council Newton Fund (215829867), administered by the University of Birmingham. We are grateful to Kelly Chance from the Harvard-Smithsonian Center for Astrophysics, the Harvard University GEOS-Chem group who maintains the model, and to Rolf Sander for maintaining the CAABA/MECCA box model.

Author contributions. L.S. and P.I.P designed the computational experiments; P.I.P. and L.S. wrote the paper; G.G.A. provided input on the paper regarding the OMI data analysis.

References

Abbot, D. S., Palmer, P. I., Martin, R. V., Chance, K. V., Jacob, D. J., and Guenther, A.: Seasonal and interannual variability of North American isoprene emissions as determined by formaldehyde column measurements from space, Geophysical Research Letters, 30, doi:10.1029/2003GL017336, http://dx.doi.org/10.1029/2003GL017336, 1886, 2003.

Barkley, M. P., Palmer, P. I., Kuhn, U., Kesselmeier, J., Chance, K., Kurosu, T. P., Martin, R. V., Helmig, D., and Guenther, A.: Net ecosystem fluxes of isoprene over tropical South America inferred from Global Ozone Monitoring Experiment (GOME) observations of HCHO columns, Journal of Geophysical Research: Atmospheres, 113, doi:10.1029/2008JD009863, http://dx.doi.org/10.1029/2008JD009863, d20304, 2008.

Barkley, M. P., Palmer, P. I., De Smedt, I., Karl, T., Guenther, A., and Van Roozendael, M.: Regulated large-scale annual shutdown of Amazonian isoprene emissions?, Geophysical Research Letters, 36, doi:10.1029/2008GL036843, 2009.

Barkley, M. P., De Smedt, I., Van Roozendael, M., Kurosu, T. P., Chance, K., Arneth, A., Hagberg, D., Guenther, A., Paulot, F., Marais, E., and Mao, J.: Top-down isoprene emissions over tropical South America inferred from SCIAMACHY and OMI formaldehyde columns, Journal of Geophysical Research: Atmospheres, 118, 6849–6868, doi:10.1002/jgrd.50552, 2013.

Caldararu, S., Palmer, P. I., and Purves, D. W.: Inferring Amazon leaf demography from satellite observations of leaf area index, Biogeosciences, 9, 1389–1404, doi:10.5194/bg-9-1389-2012, https://www.biogeosciences.net/9/1389/2012/, 2012.

Caldararu, S., Purves, D. W., and Palmer, P. I.: Phenology as a strategy for carbon optimality: a global model, Biogeosciences, 11, 763–778, doi:10.5194/bg-11-763-2014, https://www.biogeosciences.net/11/763/2014/, 2014.

Carter, W.: Documentation of the SAPRC-99 Chemical Mechanism for VOC Reactivity Assessment, 2000.

Chance, K., Palmer, P. I., Spurr, R. J. D., Martin, R. V., Kurosu, T. P., and Jacob, D. J.: Satellite observations of formaldehyde over North America from GOME, Geophysical Research Letters, 27, 3461–3464, doi:10.1029/2000GL011857, http://dx.doi.org/10.1029/2000GL011857, 2000.

Cohen, A. J., Brauer, M., Burnett, R., Anderson, H. R., Frostad, J., Estep, K., Balakrishnan, K., Brunekreef, B., Dandona, L., Dandona, R., Feigin, V., Freedman, G., Hubbell, B., Jobling, A., Kan, H., Knibbs, L., Liu, Y., Martin, R., Morawska, L., Pope, C. A., Shin, H., Straif, K., Shaddick, G., Thomas, M., van Dingenen, R., van Donkelaar, A., Vos, T., Murray, C. J. L., and Forouzanfar, M. H.: Estimates and 25-year trends of the global burden of disease attributable to ambient air pollution: an analysis of data from the Global Burden of Diseases Study 2015, The Lancet, 389, 1907 – 1918, doi:https://doi.org/10.1016/S0140-6736(17)30505-6, http://www.sciencedirect.com/science/article/pii/S0140673617305056, 2017.

Curci, G., Palmer, P. I., Kurosu, T. P., Chance, K., and Visconti, G.: Estimating European volatile organic compound emissions using satellite observations of formaldehyde from the Ozone Monitoring Instrument, Atmospheric Chemistry and Physics, 10, 11 501–11 517, doi:10.5194/acp-10-11501-2010, https://www.atmos-chem-phys.net/10/11501/2010/, 2010.

De Smedt, I., Müller, J.-F., Stavrakou, T., van der A, R., Eskes, H., and Van Roozendael, M.: Twelve years of global observations of formaldehyde in the troposphere using GOME and SCIAMACHY sen-

sors, Atmospheric Chemistry and Physics, 8, 4947–4963, doi:10.5194/acp-8-4947-2008, https://www.atmos-chem-phys.net/8/4947/2008/, 2008.

De Smedt, I., Stavrakou, T., Müller, J.-F., van der A, R. J., and Van Roozendael, M.: Trend detection in satellite observations of formaldehyde tropospheric columns, Geophysical Research Letters, 37, doi:10.1029/2010GL044245, http://dx.doi.org/10.1029/2010GL044245, l18808, 2010.

De Smedt, I., Stavrakou, T., Hendrick, F., Danckaert, T., Vlemmix, T., Pinardi, G., Theys, N., Lerot, C., Gielen, C., Vigouroux, C., Hermans, C., Fayt, C., Veefkind, P., Müller, J.-F., and Van Roozendael, M.: Diurnal, seasonal and long-term variations of global formaldehyde columns inferred from combined OMI and GOME-2 observations, Atmospheric Chemistry and Physics, 15, 12 519–12 545, doi:10.5194/acp-15-12519-2015, http://www.atmos-chem-phys.net/15/12519/2015/, 2015.

Eastham, S. D., Weisenstein, D. K., and Barrett, S. R.: Development and evaluation of the unified tropospheric–stratospheric chemistry extension (UCX) for the global chemistry-transport model GEOS-Chem, Atmospheric Environment, 89, 52 – 63, doi:10.1016/j.atmosenv.2014.02.001, 2014.

Friedl, M. A., Sulla-Menashe, D., Tan, B., Schneider, A., Ramankutty, N., Sibley, A., and Huang, X.: MODIS Collection 5 global land cover: Algorithm refinements and characterization of new datasets, Remote Sensing of Environment, 114, 168–182, doi:10.1016/j.rse.2009.08.016, 2010.

Fu, T.-M., Jacob, D. J., Palmer, P. I., Chance, K., Wang, Y. X., Barletta, B., Blake, D. R., Stanton, J. C., and Pilling, M. J.: Space-based formaldehyde measurements as constraints on volatile organic compound emissions in east and south Asia and implications for ozone, Journal of Geophysical Research: Atmospheres, 112, doi:10.1029/2006JD007853, http://dx.doi.org/10.1029/2006JD007853, d06312, 2007.

González Abad, G., Liu, X., Chance, K., Wang, H., Kurosu, T. P., and Suleiman, R.: Updated Smithsonian Astrophysical Observatory Ozone Monitoring Instrument (SAO OMI) formaldehyde retrieval, Atmospheric Measurement Techniques, 8, 19–32, doi:10.5194/amt-8-19-2015, 2015.

Gonzi, S., Palmer, P. I., Barkley, M. P., De Smedt, I., and Van Roozendael, M.: Biomass burning emission estimates inferred from satellite column measurements of HCHO: Sensitivity to co-emitted aerosol and injection height, Geophysical Research Letters, 38, doi:10.1029/2011GL047890, http://dx.doi.org/10.1029/2011GL047890, l14807, 2011.

Guenther, A. B., Jiang, X., Heald, C. L., Sakulyanontvittaya, T., Duhl, T., Emmons, L. K., and Wang, X.: The Model of Emissions of Gases and Aerosols from Nature version 2.1 (MEGAN2.1): an extended and updated framework for modeling biogenic emissions, Geoscientific Model Development, 5, 1471–1492, doi:10.5194/gmd-5-1471-2012, 2012.

Jaeglé, L., Jacob, D. J., Wang, Y., Weinheimer, A. J., Ridley, B. A., Campos, T. L., Sachse, G. W., and Hagen, D. E.: Sources and chemistry of NOx in the upper troposphere over the United States, Geophysical Research Letters, 25, 1705–1708, doi:10.1029/97GL03591, http://dx.doi.org/10.1029/97GL03591, 1998.

Justice, C., Giglio, L., Korontzi, S., Owens, J., Morisette, J., Roy, D., Descloitres, J., Alleaume, S., Petitcolin, F., and Kaufman, Y.: The MODIS fire products, Remote Sensing of Environment, 83, 244 – 262, doi:https://doi.org/10.1016/S0034-4257(02)00076-7, http://www.sciencedirect.com/science/article/pii/S0034425702000767, the Moderate Resolution Imaging Spectroradiometer (MODIS): a new generation of Land Surface Monitoring, 2002.

Kurokawa, J., Ohara, T., Morikawa, T., Hanayama, S., Janssens-Maenhout, G., Fukui, T., Kawashima, K., and Akimoto, H.: Emissions of air pollutants and greenhouse gases over Asian regions during 2000-2008: Regional Emission inventory in ASia (REAS) version 2, Atmospheric Chemistry and Physics, 13, 11 019–11 058, doi:10.5194/acp-13-11019-2013, 2013.

Levelt, P. F., van den Oord, G. H. J., Dobber, M. R., Mälkki, A., Visser, H., de Vries, J., Stammes, P., Lundell, J. O. V., and Saari, H.: The Ozone Monitoring Instrument, IEEE Transactions on Geoscience and Remote Sensing, 44, 1093–1101, 2006.

Li, M., Zhang, Q., Kurokawa, J.-I., Woo, J.-H., He, K., Lu, Z., Ohara, T., Song, Y., Streets, D. G., Carmichael, G. R., Cheng, Y., Hong, C., Huo, H., Jiang, X., Kang, S., Liu, F., Su, H., and Zheng, B.: MIX: a mosaic Asian anthropogenic emission inventory under the international collaboration framework of the MICS-Asia and HTAP, Atmospheric Chemistry and Physics, 17, 935–963, doi:10.5194/acp-17-935-2017, 2017.

Lin, Y. C., Schwab, J. J., Demerjian, K. L., Bae, M.-S., Chen, W.-N., Sun, Y., Zhang, Q., Hung, H.-M., and Perry, J.: Summertime formaldehyde observations in New York City: Ambient levels, sources and its contribution to HOx radicals, Journal of Geophysical Research: Atmospheres, 117, doi:10.1029/2011JD016504, http://dx.doi.org/10.1029/2011JD016504, d08305, 2012.

Lu, Z. and Streets, D. G.: Increase in NOx Emissions from Indian Thermal Power Plants during 1996–2010: Unit-Based Inventories and Multisatellite Observations, Environmental Science & Technology, 46, 7463–7470, doi:10.1021/es300831w, 2012.

Lu, Z., Zhang, Q., and Streets, D. G.: Sulfur dioxide and primary carbonaceous aerosol emissions in China and India, 1996-2010, Atmospheric Chemistry and Physics, 11, 9839–9864, doi:10.5194/acp-11-9839-2011, 2011.

Mahajan, A. S., Smedt, I. D., Biswas, M. S., Ghude, S., Fadnavis, S., Roy, C., and van Roozendael, M.: Inter-annual variations in satellite observations of nitrogen dioxide and formaldehyde over India, Atmospheric Environment, 116, 194 – 201, doi:10.1016/j.atmosenv.2015.06.004, 2015.

Marais, E. A., Jacob, D. J., Kurosu, T. P., Chance, K., Murphy, J. G., Reeves, C., Mills, G., Casadio, S., Millet, D. B., Barkley, M. P., Paulot, F., and Mao, J.: Isoprene emissions in Africa inferred from OMI observations of formaldehyde columns, Atmospheric Chemistry and Physics, 12, 6219–6235, doi:10.5194/acp-12-6219-2012, 2012.

Martin, R. V., Jacob, D. J., Chance, K., Kurosu, T. P., Palmer, P. I., and Evans, M. J.: Global inventory of nitrogen oxide emissions constrained by space-based observations of NO2 columns, Journal of Geophysical Research: Atmospheres, 108, doi:10.1029/2003JD003453, 2003.

Marvin, M. R., Wolfe, G. M., Salawitch, R. J., Canty, T. P., Roberts, S. J., Travis, K. R., Aikin, K. C., de Gouw, J. A., Graus, M., Hanisco, T. F., Holloway, J. S., Hübler, G., Kaiser, J., Keutsch, F. N., Peischl, J., Pollack, I. B., Roberts, J. M., Ryerson, T. B., Veres, P. R., and Warneke, C.: Impact of evolving isoprene mechanisms on simulated formaldehyde: An inter-comparison supported by in situ observations from SENEX, Atmospheric Environment, 164, 325 – 336, doi:10.1016/j.atmosenv.2017.05.049, 2017.

Millet, D. B., Jacob, D. J., Boersma, K. F., Fu, T.-M., Kurosu, T. P., Chance, K., Heald, C. L., and Guenther, A.: Spatial distribution of isoprene emissions from North America derived from formaldehyde column measurements by the OMI satellite sensor, Journal of Geophysical Research: Atmospheres, 113, doi:10.1029/2007JD008950, http://dx.doi.org/10.1029/2007JD008950, d02307, 2008.

Pai, D. S. and Bhan, S. C.: Monsoon 2014 A Report, Tech. Rep. ESSO/IMD/Synoptic Met./01(2015)/17, India Meteorological Department, 2015.

Palmer, P. I., Jacob, D. J., Chance, K., Martin, R. V., Spurr, R. J. D., Kurosu, T. P., Bey, I., Yantosca, R., Fiore, A., and Li, Q.: Air mass factor formulation for spectroscopic measurements from satellites: Application to formaldehyde retrievals from the Global Ozone Monitoring Experiment, Journal of Geophysical Research: Atmospheres, 106, 14 539–14 550, doi:10.1029/2000JD900772, 2001.

Palmer, P. I., Jacob, D. J., Fiore, A. M., Martin, R. V., Chance, K., and Kurosu, T. P.: Mapping isoprene emissions over North America using formaldehyde column observations from space, Journal of Geophysical Research: Atmospheres, 108, doi:10.1029/2002JD002153, 2003.

Palmer, P. I., Abbot, D. S., Fu, T.-M., Jacob, D. J., Chance, K., Kurosu, T. P., Guenther, A., Wiedinmyer, C., Stanton, J. C., Pilling, M. J., Pressley, S. N., Lamb, B., and Sumner, A. L.: Quantifying the seasonal and interannual variability of North American isoprene emissions using satellite observations of the formaldehyde column, Journal of Geophysical Research: Atmospheres, 111, doi:10.1029/2005JD006689, 2006.

Palmer, P. I., Barkley, M. P., Kurosu, T. P., Lewis, A. C., Saxton, J. E., Chance, K., and Gatti, L. V.: Interpreting satellite column observations of formaldehyde over tropical South America, Philosophical Transactions of the Royal Society of London A: Mathematical, Physical and Engineering Sciences, 365, 1741–1751, doi:10.1098/rsta.2007.2042, http://rsta.royalsocietypublishing.org/content/365/1856/1741, 2007.

Perianayagam, A. and Goli, S.: Provisional results of the 2011 Census of India: Slowdown in growth, ascent in literacy, but more missing girls, International Journal of Social Economics, 39, 785–801, doi:10.1108/03068291211253395, 2012.

Sander, R., Baumgaertner, A., Gromov, S., Harder, H., Jöckel, P., Kerkweg, A., Kubistin, D., Regelin, E., Riede, H., Sandu, A., Taraborrelli, D., Tost, H., and Xie, Z.-Q.: The atmospheric chemistry box model CAABA/MECCA-3.0, Geoscientific Model Development, 4, 373–380, doi:10.5194/gmd-4-373-2011, 2011.

Sander, R., Jöckel, P., Kirner, O., Kunert, A. T., Landgraf, J., and Pozzer, A.: The photolysis module JVAL-14, compatible with the MESSy standard, and the JVal PreProcessor (JVPP), Geoscientific Model Development, 7, 2653–2662, doi:10.5194/gmd-7-2653-2014, https://www.geosci-model-dev.net/7/2653/2014/, 2014.

Santenda and Kaushik, A. D.: Forest Fire Disaster Management, Tech. rep., Institute of Disaster Management, Ministry of Home Affairs, New Delhi, iSBN-978-93-82571-09-4, 2014.

Sharma, S., Chatani, S., Mahtta, R., Goel, A., and Kumar, A.: Sensitivity analysis of ground level ozone in India using WRF-CMAQ models, Atmospheric Environment, 131, 29 – 40, doi:https://doi.org/10.1016/j.atmosenv.2016.01.036, http://www.sciencedirect.com/science/article/pii/S1352231016300504, 2016.

Shim, C., Wang, Y., Choi, Y., Palmer, P. I., Abbot, D. S., and Chance, K.: Constraining global isoprene emissions with Global Ozone Monitoring Experiment (GOME) formaldehyde column measurements, Journal of Geophysical Research: Atmospheres, 110, doi:10.1029/2004JD005629, http://dx.doi.org/10.1029/2004JD005629, d24301, 2005.

Singaas, E. L., Lerdau, M., Winter, K., and Sharkey, T. D.: Isoprene increases thermotolerance of isoprene-emitting species, Plant Physiol., pp. 1413–1420, doi:DOI:10.1104/pp.115.4.1413, 1997.

Stavrakou, T., Müller, J.-F., De Smedt, I., Van Roozendael, M., van der Werf, G. R., Giglio, L., and Guenther, A.: Global emissions of non-methane hydrocarbons deduced from SCIAMACHY formaldehyde columns

through 2003–2006, Atmospheric Chemistry and Physics, 9, 3663–3679, doi:10.5194/acp-9-3663-2009, https://www.atmos-chem-phys.net/9/3663/2009/, 2009.

Stavrakou, T., Müller, J.-F., Bauwens, M., De Smedt, I., Lerot, C., Van Roozendael, M., Clerbaux, C., Boersma, K. F., van der A, R., and Song, Y.: Substantial Underestimation of Post-Harvest Burning Emissions in the North China Plain Revealed by Multi-Species Space Observations, Nature Scientific Reports, 6, doi:10.1038/srep32307, 2016.

Taraborrelli, D., Lawrence, M. G., Butler, T. M., Sander, R., and Lelieveld, J.: Mainz Isoprene Mechanism 2 (MIM2): an isoprene oxidation mechanism for regional and global atmospheric modelling, Atmospheric Chemistry and Physics, 9, 2751–2777, doi:10.5194/acp-9-2751-2009, 2009.

Thomas, W., Hegels, E., Slijkhuis, S., Spurr, R., and Chance, K.: Detection of biomass burning combustion products in Southeast Asia from backscatter data taken by the GOME Spectrometer, Geophysical Research Letters, 25, 1317–1320, doi:10.1029/98GL01087, http://dx.doi.org/10.1029/98GL01087, 1998.

Tyagi, S., Tiwari, S., Mishra, A., Hopke, P. K., Attri, S., Srivastava, A., and Bisht, D.: Spatial variability of concentrations of gaseous pollutants across the National Capital Region of Delhi, India, Atmospheric Pollution Research, 7, 808–816, doi:10.1016/j.apr.2016.04.008, 2016.

van der Werf, G. R., Randerson, J. T., Giglio, L., van Leeuwen, T. T., Chen, Y., Rogers, B. M., Mu, M., van Marle, M. J. E., Morton, D. C., Collatz, G. J., Yokelson, R. J., and Kasibhatla, P. S.: Global fire emissions estimates during 1997–2016, Earth System Science Data, 9, 697–720, doi:10.5194/essd-9-697-2017, 2017.

Volkamer, R., Sheehy, P., Molina, L. T., and Molina, M. J.: Oxidative capacity of the Mexico City atmosphere Part 1: A radical source perspective, Atmospheric Chemistry and Physics, 10, 6969–6991, doi:10.5194/acp-10-6969-2010, https://www.atmos-chem-phys.net/10/6969/2010/, 2010.

Wang, C., Huang, X.-F., Han, Y., Zhu, B., and He, L.-Y.: Sources and Potential Photochemical Roles of Formaldehyde in an Urban Atmosphere in South China, Journal of Geophysical Research: Atmospheres, doi:10.1002/2017JD027266, http://dx.doi.org/10.1002/2017JD027266, 2017JD027266, 2017.

Whalley, L. K., Furneaux, K. L., Goddard, A., Lee, J. D., Mahajan, A., Oetjen, H., Read, K. A., Kaaden, N., Carpenter, L. J., Lewis, A. C., Plane, J. M. C., Saltzman, E. S., Wiedensohler, A., and Heard, D. E.: The chemistry of OH and HO_2 radicals in the boundary layer over the tropical Atlantic Ocean, Atmospheric Chemistry and Physics, 10, 1555–1576, doi:10.5194/acp-10-1555-2010, https://www.atmos-chem-phys.net/10/1555/2010/, 2010.

Wolfe, G. M., Kaiser, J., Hanisco, T. F., Keutsch, F. N., de Gouw, J. A., Gilman, J. B., Graus, M., Hatch, C. D., Holloway, J., Horowitz, L. W., Lee, B. H., Lerner, B. M., Lopez-Hilifiker, F., Mao, J., Marvin, M. R., Peischl, J., Pollack, I. B., Roberts, J. M., Ryerson, T. B., Thornton, J. A., Veres, P. R., and Warneke, C.: Formaldehyde production from isoprene oxidation across NO_x regimes, Atmospheric Chemistry and Physics, 16, 2597–2610, doi:10.5194/acp-16-2597-2016, https://www.atmos-chem-phys.net/16/2597/2016/, 2016.

Young, E. L. and Paton-Walsh, C.: Formaldehyde and nitrogen dioxide in smoke plumes from Australia's Black Saturday fires, IOP Conference Series: Earth and Environmental Science, 11, 012 023, http://stacks.iop.org/1755-1315/11/i=1/a=012023, 2010.

Zhu, L., Jacob, D. J., Mickley, L. J., Marais, E. A., Cohan, D. S., Yoshida, Y., Duncan, B. N., Abad, G. G., and Chance, K. V.: Anthropogenic emissions of highly reactive volatile organic compounds in eastern Texas

inferred from oversampling of satellite (OMI) measurements of HCHO columns, Environmental Research Letters, 9, 114 004, 2014.

Zhu, L., Jacob, D. J., Kim, P. S., Fisher, J. A., Yu, K., Travis, K. R., Mickley, L. J., Yantosca, R. M., Sulprizio, M. P., De Smedt, I., González Abad, G., Chance, K., Li, C., Ferrare, R., Fried, A., Hair, J. W., Hanisco, T. F., Richter, D., Jo Scarino, A., Walega, J., Weibring, P., and Wolfe, G. M.: Observing atmospheric formaldehyde (HCHO) from space: validation and intercomparison of six retrievals from four satellites (OMI, GOME2A, GOME2B, OMPS) with SEAC^{4}RS aircraft observations over the southeast US, Atmospheric Chemistry and Physics, 16, 13 477–13 490, doi:10.5194/acp-16-13477-2016, https://www.atmos-chem-phys.net/16/13477/2016/, 2016.

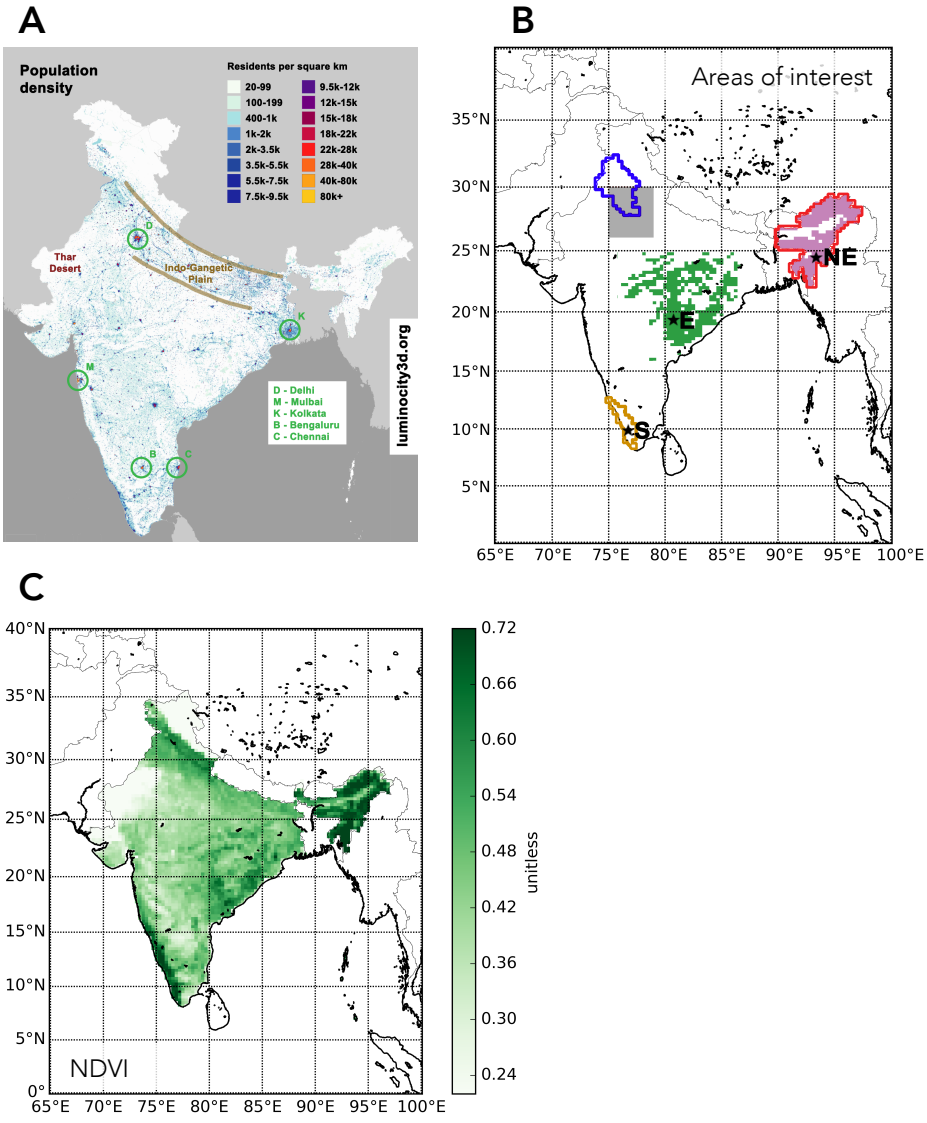

Figure 1: Geography of India: population density based on the 2001 census (top left); focal points of this study (top right); and annual mean values of the Normalized Difference Vegetation Index (NDVI) for 2014 from the NASA MODIS instrument, averaged on the $0.25° \times 0.3125°$ GEOS-Chem nested grid. For the map of focal points: the blue outline represent the states of Punjab and Haryana; the red outline denotes Seven sister states; and the yellow outline represents the state of Kerala. The pink and green shaded areas denote the NE and E forest sites, where we infer isoprene emissions from OMI HCHO columns. The grey shaded area ~~denote~~ denotes the oversampling region used to study Delhi. The stars denote the sites where we study HCHO production using a 0-D photochemical model. The population image is ~~taken~~ modified with permission from ~~Wikimedia c/o CC-by-sa PlaneMad/Wikimedia~~LuminoCity3D.org: data provided by EC JRC & CIESIN, and the design provided by D. A. Smith, Barlett Centre for Advanced Spatial Analysis, University College London.

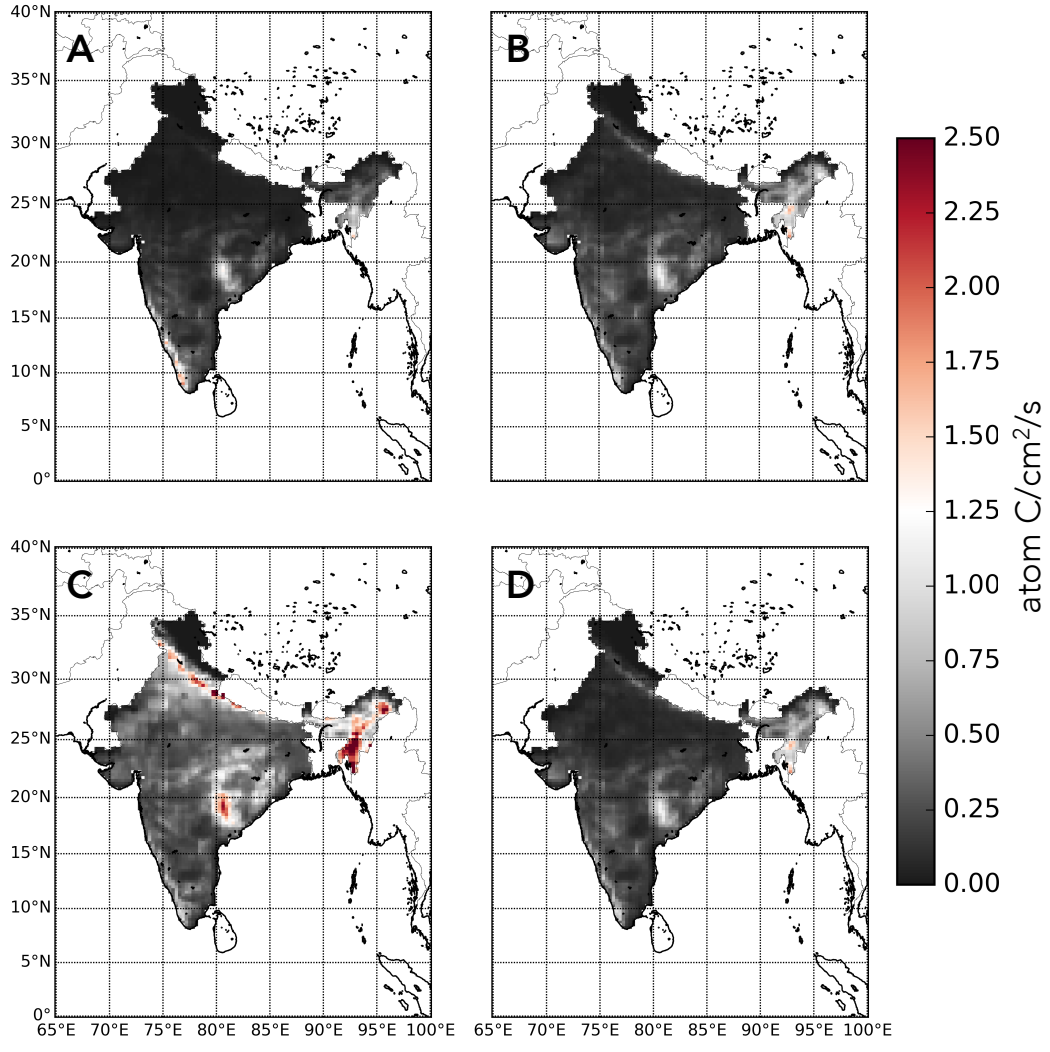

Figure 2: Seasonal isoprene emission rates (atom C/cm^2/s) from the MEGAN inventory (Guenther et al., 2012). Data are described on the GEOS-Chem $0.25° \times 0.3125°$ grid for A) winter (JF), B) pre-monsoon (MAM), C) monsoon (JJAS), and D) post-monsoon seasons (OND).

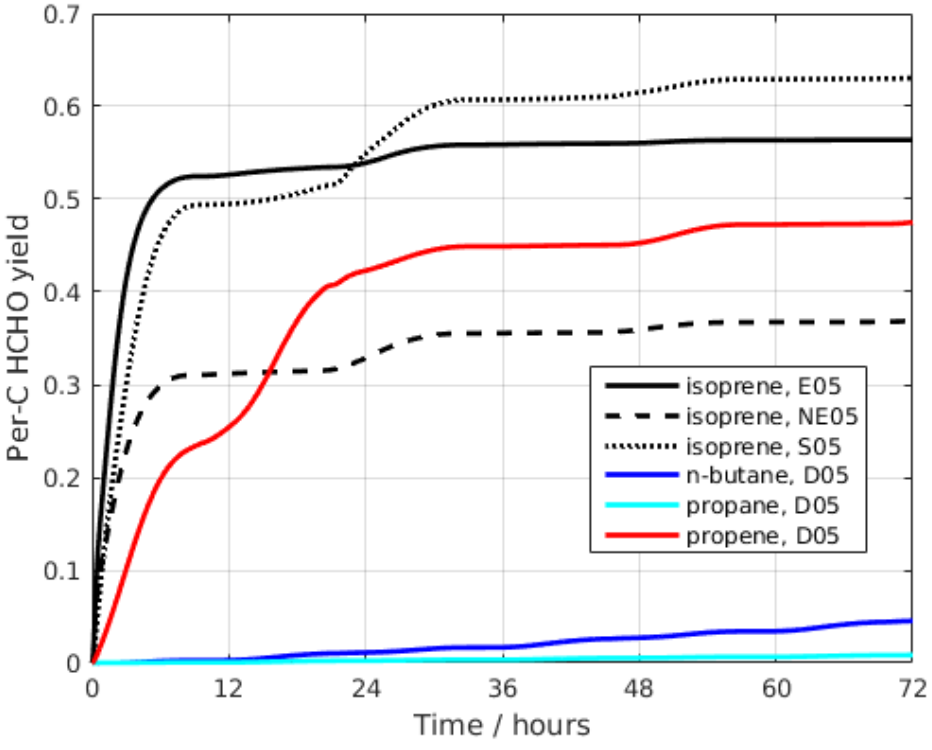

Figure 3: Time-dependent cumulative HCHO yield (~~per unit C~~per-C) produced from isoprene in three contrasting photochemical environments, and from propene, propane, and n-butane in an urban photochemical environments based on Delhi. Calculations are denoted by an alphanumeric code that is explained in Table 1.

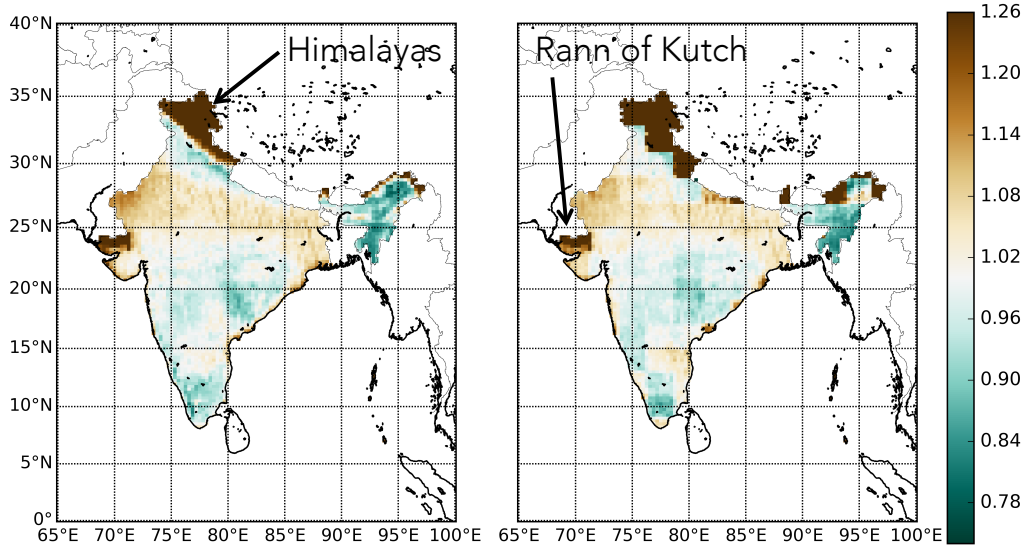

Figure 4: Annual mean air mass factors (AMFs) for 2014 calculated using (left) nested $0.25° \times 0.3125°$ and (right) standard $2.0° \times 2.5°$ GEOS-Chem grid.

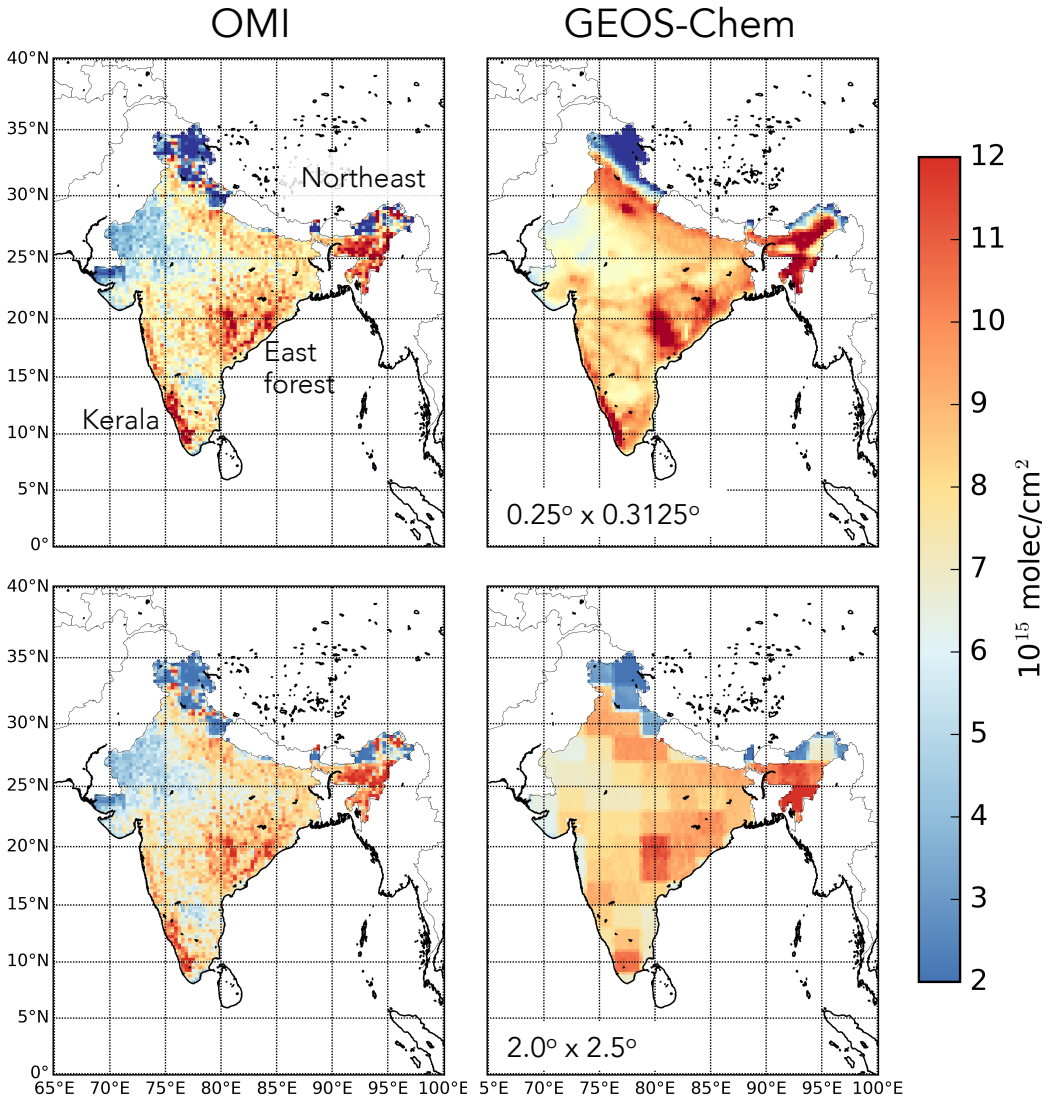

Figure 5: Annual mean clear-sky (left) OMI and (right) GEOS-Chem HCHO vertical columns (10^{15}molec/cm^2) over India for 2014. The OMI vertical columns are described on the $0.25° \times 0.3125°$ GEOS-Chem grid. These vertical columns are transformed from observed slant columns using AMFs informed by the distribution of HCHO described by the (top) nested $0.25° \times 0.3125°$ and (bottom) standard $2.0° \times 2.5°$ GEOS-Chem grid. Data exclusion criteria are described in the main text. The model is sampled at the time and location of each observed scene.

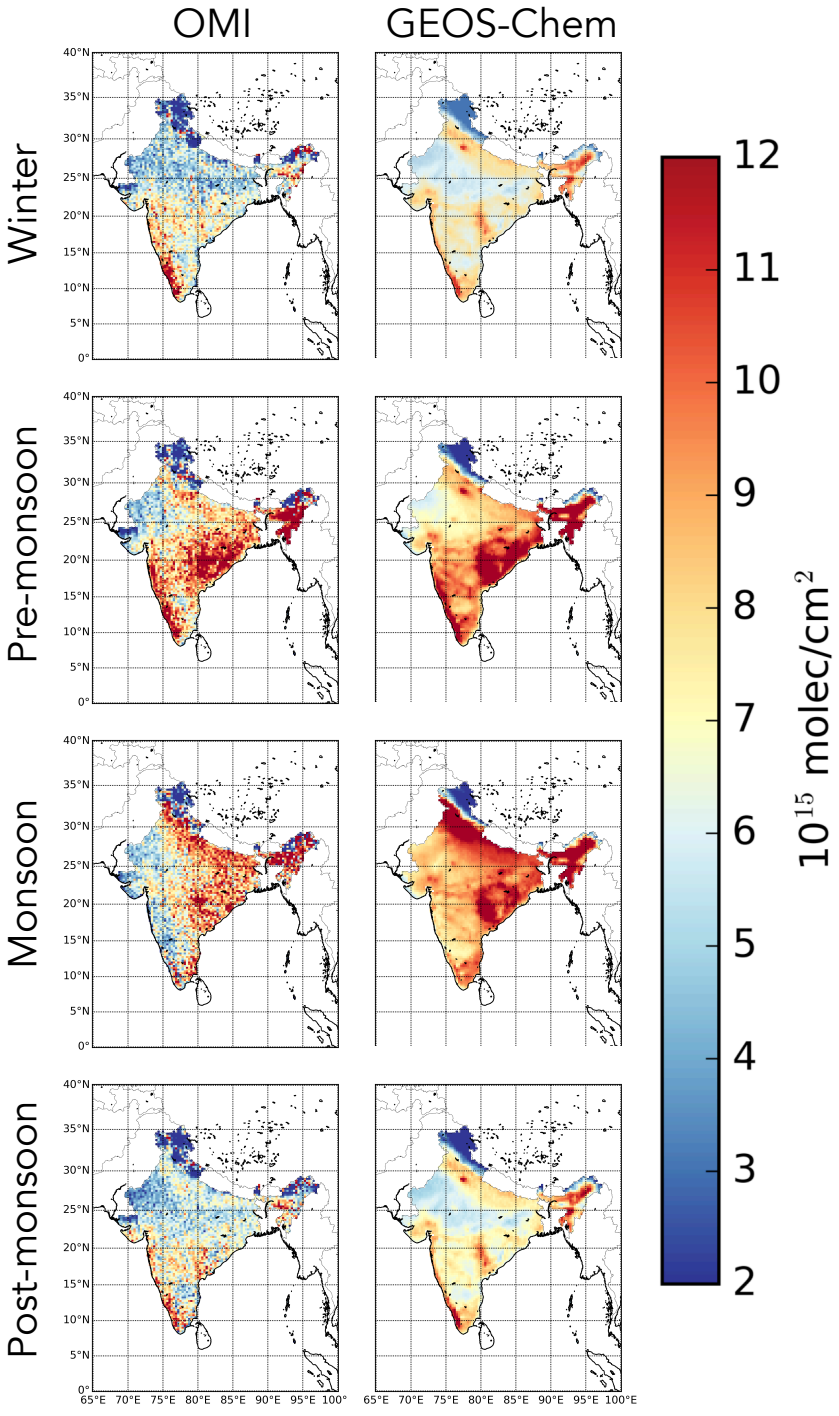

Figure 6: Seasonal mean clear-sky (left) OMI and (right) GEOS-Chem HCHO vertical columns (10^{15}molec/cm^2) for 2014, averaged on a common $0.25° \times 0.3125°$ grid. Seasonal definitions are described in Section 2.

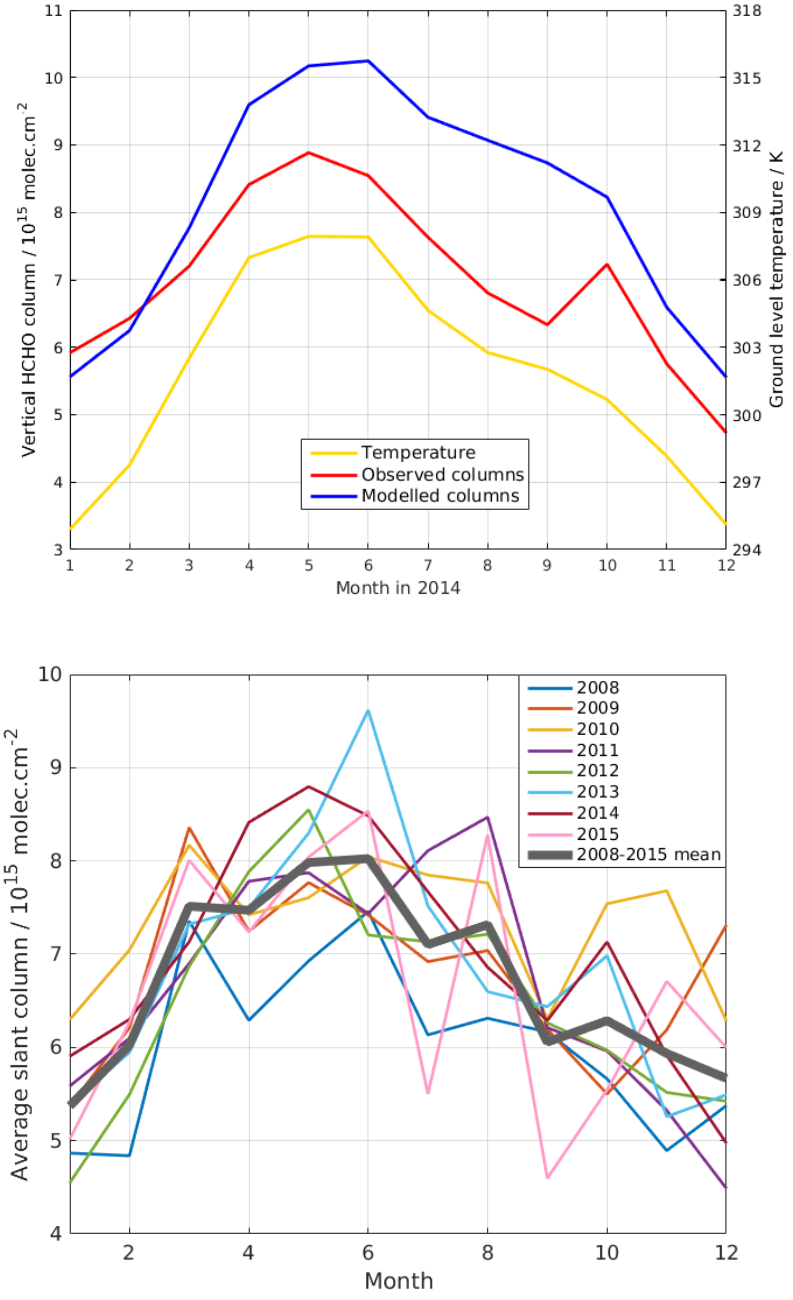

Figure 7: Timeseries of (top) OMI and GEOS-Chem vertical columns (10^{15} molec/cm^2) for 2014, and (bottom) OMI slant columns (10^{15} molec/cm^2) from 2008 to 2015 over India. GEOS-FP ground-level temperature (K) is also shown in the ~~left~~ top panel. The thick grey line in the ~~right~~ bottom panel denotes 2008–2015 HCHO column monthly means.

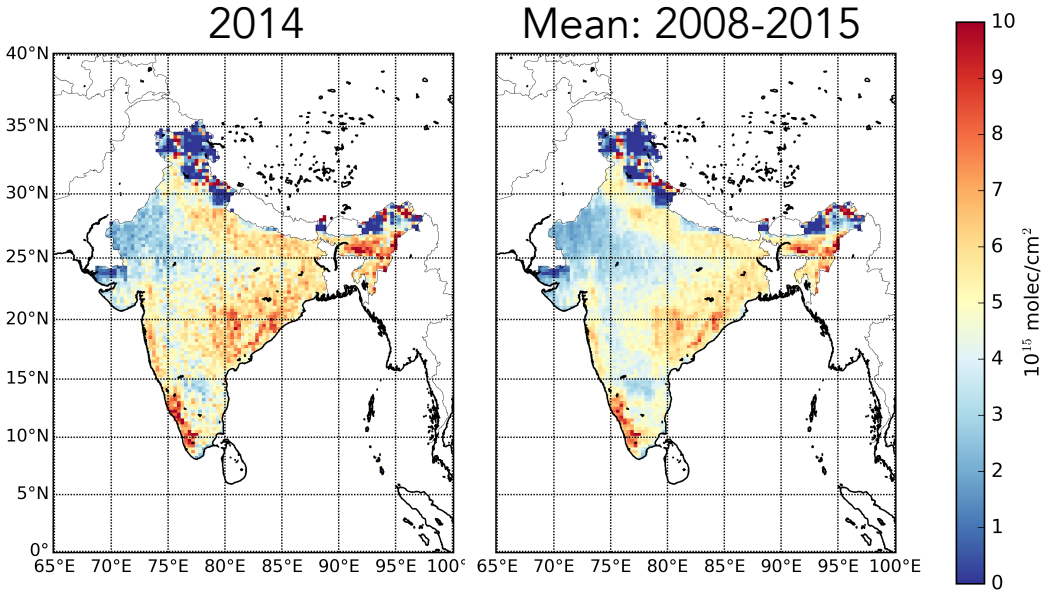

Figure 8: Annual mean OMI HCHO slant columns (10^{15}molec/cm^2) over India for (left) 2014 and (right) 2008–2015, averaged on a common $0.25° \times 0.3125°$ grid.

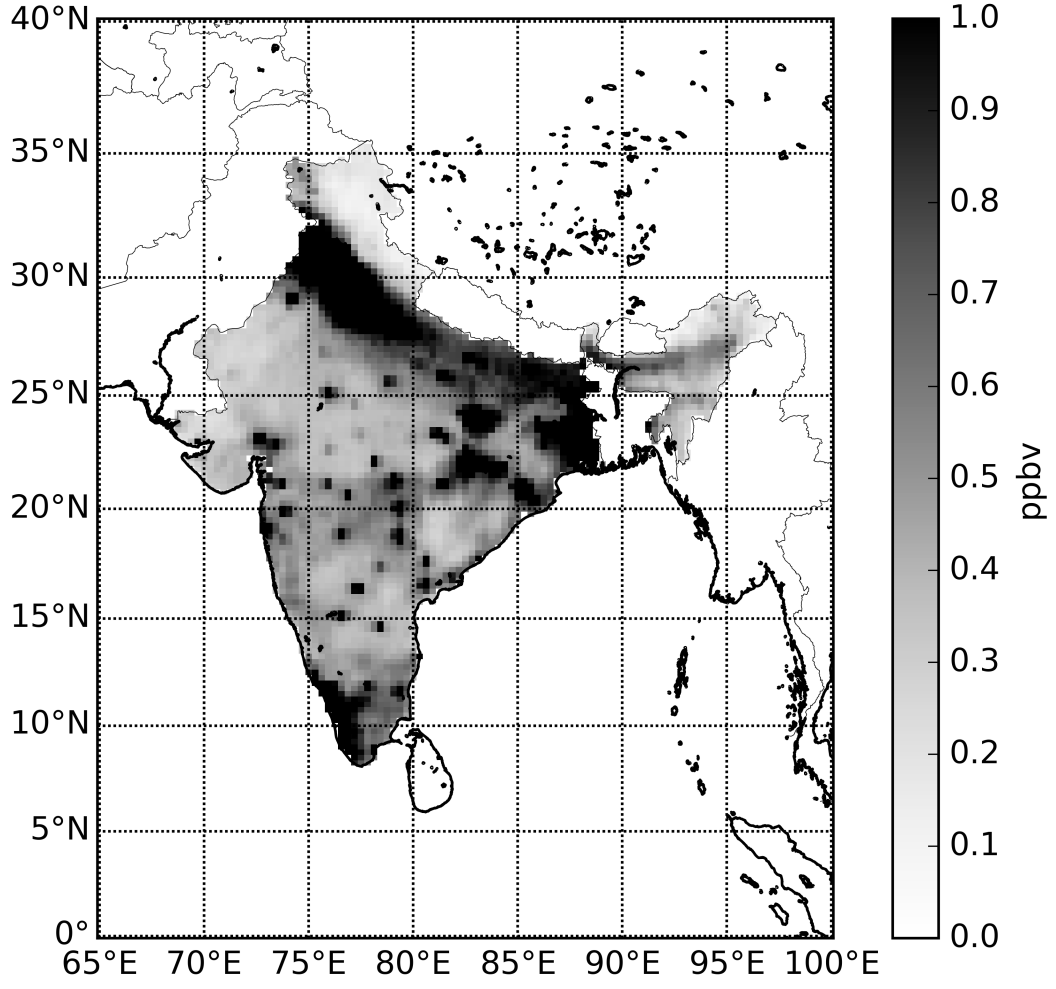

Figure 9: Annual mean GEOS-Chem ground-level NO_x mixing ratios (ppbv) in 2014, averaged on the $0.25° \times 0.3125°$ grid.

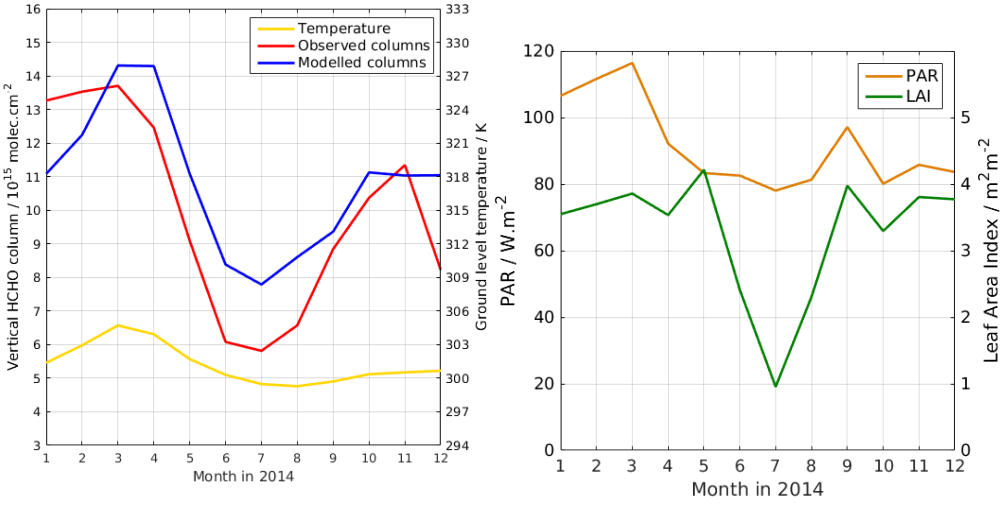

Figure 10: Timeseries of (left) monthly mean OMI and GEOS-Chem vertical HCHO columns (10^{15}molec/cm^2), and GEOS-FP ground-level temperature, and (right) PAR (W/m^2) and LAI (m^2/m^2) over the state of Kerala in 2014.

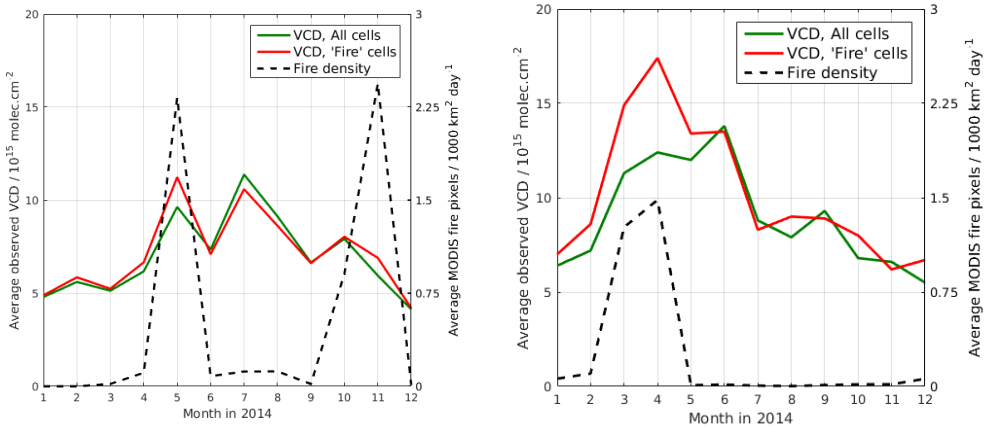

Figure 11: Timeseries of monthly mean HCHO columns (10^{15}molec/cm^2) and the number of MODIS fire detections (10^3 km^2/day) over (left) the states of Punjab and Haryana and (right) North-eastern India. The green line denotes all HCHO columns over the region, and the red line denotes columns that are most affected by fires as indicated by MODIS firecounts.

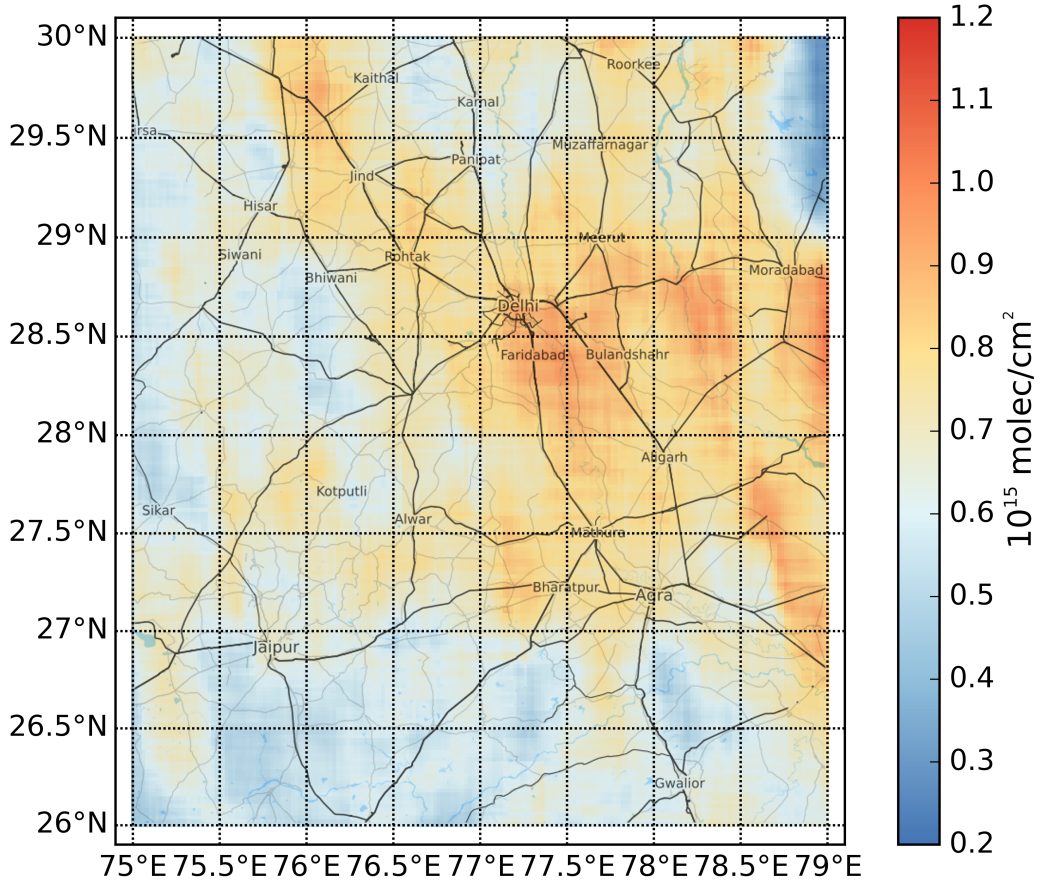

Figure 12: Oversampled distribution of OMI vertical HCHO columns (10^{15}molec/cm^2) around Delhi. ~~Underlying map imagery~~ The underlying road network is ~~taken~~ reproduced with permission from © www.thunderforest.com (map) and from © www.osm.org/copyright (data).

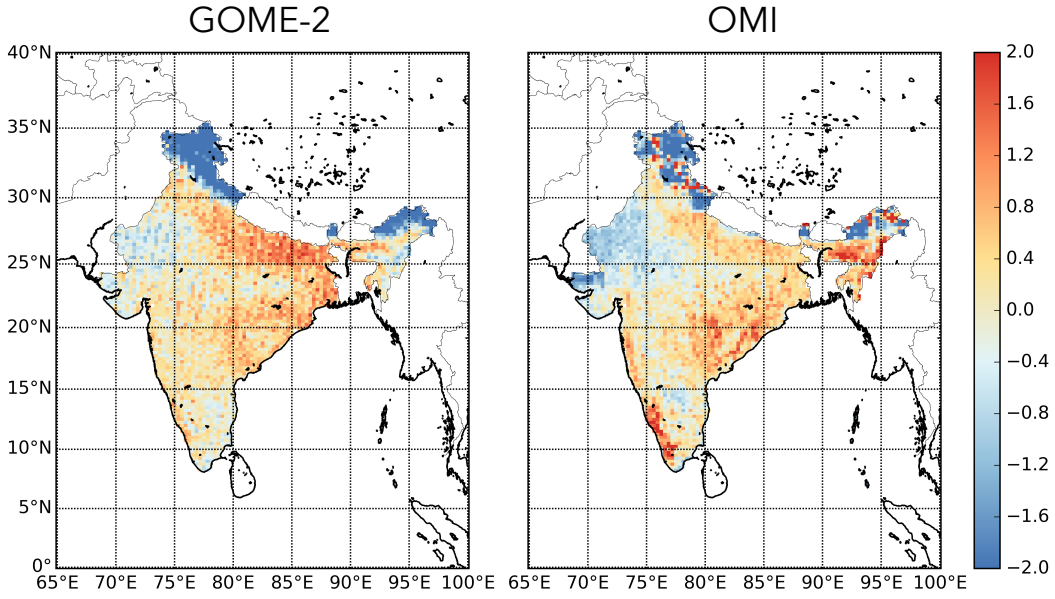

Figure 13: Standardized HCHO slant columns for 2014 (unitless) from (left) the Global Ozone Monitoring Experiment-2 (GOME-2) aboard MetOp and (right) OMI, averaged on a common $0.25° \times 0.3125°$ grid. GOME-2 and OMI have local equatorial overpass times of 0930 and 1330, respectively.

Table 1: Photochemical and meteorological scenarios used for box model calculations. The emboldened letters E, NE, S denote the forested regions (Figure 1) and D denotes Delhi. Ground-level temperature (T), relative humidity (RH), ~~and~~ boundary layer height ~~are denoted by T, RH, and~~ (BLH) and mixing ratios are GEOS-Chem monthly mean values from each location.

Scenario name	Location	Month of year	T [K]	RH [%]	BLH [m]	Fixed mixing ratio [ppbv]		
						O_3	CO	NO_2
E01	**E** 19.3°N 80.6°E	Jan	295	56	1240	49	232	1.1
E05		May	307	33	1873	63	131	2.4
E08		Aug	299	84	685	39	114	1.3
E11		Nov	304	64	611	49	220	0.8
NE01	**NE** 24.4°N 93.1°E	Jan	292	65	648	42	277	1.8
NE05		May	302	59	1202	55	154	0.8
NE08		Aug	299	88	666	24	127	1.3
NE11		Nov	296	73	925	43	241	1.4
S01	**S** 9.8°N 76.6°E	Jan	300	59	1090	48	260	8.9
S05		May	301	78	725	32	146	8.6
S08		Aug	299	84	690	18	122	8.1
S11		Nov	299	77	732	45	274	8.9
D05	**D** 28.61°N 77.23°E	May	307	18	1975	37	2300	19

Table 2: Results of the photochemical box modelling for forested region scenarios (Table 1).

Scenario	Isoprene lifetime [min]	Time to reach peak HCHO signal [min]	HCHO yield [~~per unit C~~per-C]
E01	26	79	0.50
E05	14	59	0.55
E08	10	33	0.49
E11	20	83	0.41
NE01	28	89	0.59
NE05	10	33	0.38
NE08	10	33	0.58
NE11	18	57	0.53
S01	64	127	0.63
S05	48	147	0.63
S08	70	189	0.66
S11	52	153	0.62

Table 3: *A priori* and *a posteriori* isoprene emission estimates (10^{11} atom C/cm^2/s) over NE and E forest sites (Figure 1), and the model linear regression coefficients that relate model isoprene emissions and HCHO columns.

Season	Mean *a priori* emission [10^{11} atom C/cm^2/s]	Slope S [10^3 s]	Intercept Ω_b [10^{15} molec/cm^2]	r^2	Mean *a posteriori* emission [10^{11} atom C/cm^2/s]	% change from *a priori*
East Forest Region						
Winter	2.8	4.1	5.3	0.59	3.0	+7
Pre-monsoon	10.2	4.3	7.0	0.67	7.8	-24
Monsoon	7.4	4.3	7.6	0.51	3.3	-55
Post-monsoon	3.6	4.9	5.2	0.47	2.6	-28
Northeast Forest Region						
Winter	3.5	3.9	3.9	0.42	4.4	+26
Pre-monsoon	17.9	2.9	6.2	0.58	12.6	-30
Monsoon	14.6	2.2	8.7	0.27	1.7	-88
Post-monsoon	6.6	4.9	5.1	0.49	2.7	-59